A dynamic rRNA ribomethylome drives stemness in acute myeloid leukemia

Fengbiao Zhou[1,2,14,*], Nesrine Aroua[3,4,14], Yi Liu[1,2], Christian Rohde[1,2], Jingdong Cheng[5], Anna-Katharina Wirth[6], Daria Fijalkowska[7], Stefanie Göllner[1], Michelle Lotze[1], Haiyang Yun[1], Xiaobing Yu[1], Caroline Pabst[1], Tim Sauer[1], Thomas Oellerich[8], Hubert Serve[8], Christoph Röllig[9], Martin Bornhäuser[9], Christian Thiede[9], Claudia Baldus[10], Michaela Frye[11], Simon Raffel[1], Jeroen Krijgsveld[7], Irmela Jeremias[6,12], Roland Beckmann[5], Andreas Trumpp[3,4,13,*], Carsten Müller-Tidow[1,2,13,*]

[1]Department of Internal Medicine V, Heidelberg University Hospital, 69120 Heidelberg; [2]Molecular Medicine Partnership Unit EMBL-UKHD, 69120 Heidelberg; [3]Division of Stem Cells and Cancer, German Cancer Research Center (DKFZ), 69120 Heidelberg; [4]Heidelberg Institute of Stem Cell Technology and Experimental Medicine (HI-STEM gGmbH); [5]Gene Center, Department of Biochemistry, University of Munich, 81377 Munich, Germany; [6]Research Unit Apoptosis in Hematopoietic Stem Cells (AHS), Helmholtz Center Munich, German Center for Environmental Health, 81377 Munich; [7]Division of Proteomics of Stem Cells and Cancer, German Cancer Research Center (DKFZ), 69120 Heidelberg; [8]Department of Medicine II, Hematology/Oncology, Goethe University, Frankfurt Am Main 60590; [9]Medical Department 1, University Hospital Dresden, 01307 Dresden; [10]Department of Medicine II, Hematology and Oncology, University Hospital Schleswig-Holstein, 24098 Kiel. [11]Division of Mechanisms Regulating Gene Expression, German Cancer Research Center (DKFZ), 69120 Heidelberg; [12]German Cancer Consortium (DKTK), Partner Site Munich, Munich, Germany; [13]National Center for Tumor Diseases, NCT Heidelberg, 69120 Heidelberg; [14]These authors contributed equally to this work. [*]Corresponding authors.

Running title: rRNA 2'-O-methylation regulates leukemic self-renewal.

Corresponding authors: Fengbiao Zhou, Department of Internal Medicine V, Heidelberg University Hospital, 69120 Heidelberg, Fengbiao.Zhou@med.uni-heidelberg.de, +49-(0)6221-56-37487; Andreas Trumpp, Division of Stem Cells and Cancer, German Cancer Research Center (DKFZ), 69120 Heidelberg, a.trumpp@dkfz.de, +49-(0)6221-42-3901; Carsten Müller-Tidow, Department of Internal Medicine V, Heidelberg University Hospital, 69120 Heidelberg, Carsten.Mueller-Tidow@med.uni-heidelberg.de, +49-(0)6221-56-8000.

The authors declare no potential conflicts of interest.

Abstract

The development and regulation of malignant self-renewal remains an unresolved issue. Here, we provide biochemical, genetic, and functional evidence that dynamics in ribosomal RNA (rRNA) 2'-O-methylation regulate leukemia stem cell (LSC) activity *in vivo*. A comprehensive analysis of the rRNA 2'-O-methylation landscape of 94 acute myeloid leukemia (AML) patients revealed dynamic 2'-O-methylation

specifically at exterior sites of ribosomes. rRNA 2'-O-methylation pattern is closely associated with AML development stage and LSC gene expression signature. Forced expression of 2'-O-methyltransferase FBL induced an AML stem cell phenotype and enabled engraftment of non-LSC leukemia cells in NSG mice. Enhanced 2'-O-methylation redirected the ribosome translation program towards amino acid transporter mRNAs enriched in optimal codons and subsequently increased intracellular amino acid levels. Methylation at the single site 18S-guanosine 1447 was instrumental for LSC activity. Collectively, our work demonstrates that dynamic 2'-O-Me at specific sites on ribosomal RNAs shifts translational preferences and controls AML-LSC self-renewal.

Significance: We establish the complete rRNA 2'-O-methylation landscape in human AML. Plasticity of rRNA 2´-O-methylation shifts protein translation towards a leukemia stem cell phenotype. This dynamic process constitutes a novel concept how cancers reprogram cell fate and function.

Introduction

Cancers are heterogenous tissues composed of cells with diverse phenotypes and states. Propagation of many cancers including AML depend on a small subset of self-renewing cells, cancer/leukemia stem cells(1). Illustration of the pathways which induce cancer stem cell phenotypes may enable development of conceptually new therapies. While self-renewal has been studied primarily and intensively at the level of epigenetics and transcription, the comprehensive repertoire of leukemia stem cell determinants remains to be fully defined. Recent studies have revealed the crucial role of post-transcriptional mechanisms in the maintenance of normal and malignant stem cells(2,3). The importance of post-transcriptional regulation is emphasized by the fact that transcription profiles often do not reflect the cellular functional proteome that ultimately defines cell identity and function(4,5). Importantly, stem cell features are closely linked with fine-tuned protein synthesis(6-9). Protein synthesis determines the switch between the quiescent and the activated state, and defines whether activated stem cells self-renew or differentiate(6-9). Specifically, maintenance of self-renewal requires the coordination of low global protein synthesis with selective translation of specific proteins crucial for stem cells, including those involved in stress adaptation and energy homeostasis(3,10,11). The molecular basis for selective translation in stem cells is largely unknown but might be linked to alterations in the translation apparatus. Mutations which affect the protein translation machinery induce dysfunction of stem cells and increased cancer susceptibility in ribosomopathy patients(12,13). For example, ribosome protein haploinsufficiency results in reduced ribosome level and translation of GATA1 mRNA, impairing erythroid lineage commitment in Diamond-Blackfan anemia (DBA) patients(12). So far, congenital ribosomal mutations in ribosomopathies and somatic ribosomal mutations in various cancers mainly affect ribosomal proteins. By contrast, cancer-related alterations in ribosomal RNA and the functional consequences of such changes have been much less studied.

One of the key features of rRNA is the high degree of peri- and post-transcriptional chemical modifications during ribosome biogenesis(14). On the molecular level, these modifications stabilize ribosome structure, optimize the interaction of ribosomes with tRNAs, mRNAs and translation factors and are supposed to be fundamental to global ribosome topology and functions(14-17). More recently, it was shown that rRNA modifications may represent an important source of ribosome heterogeneity and provide critical variables in protein expression(18,19). In humans, the most abundant rRNA modification is 2'-O-methylation which is catalyzed by the C/D box snoRNP complex which contains the methyltransferase Fibrillarin (FBL), scaffold proteins NOP58, NOP56 and NHP2L1, as well as the guiding C/D box snoRNA(20,21). Recently, we showed that C/D box snoRNA abundance is associated with leukemia stem cell frequency(22). Accordingly, C/D box snoRNAs and their directed 2'-O-Me might be involved in leukemic self-renewal(22) and cellular proliferation(23). In addition, the relevance of rRNA 2'-O-Me to human disease has also been identified and described in multiple cancer cell lines and tissues(24-28). Despite these extensive studies, the plasticity, diversity and dynamics of rRNA 2'-O-Me in human malignancies and particularly, its role in acquisition and maintenance of cancer stem cell phenotypes have remained elusive.

Acute Myeloid Leukemia (AML) is an instructive model to address these questions, since cell state diversity is an important disease hallmark of AML, which is composed of a mix of self-renewing leukemic stem cells and leukemic blasts with different stages of differentiation(1,29). Thus, exploration of rRNA modifications in AML may reveal how protein expression is regulated via ribosome heterogeneity to give rise to the remarkable diversity of cell types and to control unique cell behaviors. In this study, we performed integrated analysis of rRNA 2'-O-methylation patterns in human primary AMLs, their three-dimensional structural distribution on ribosome and the associated gene expression signatures and clinical features. We further evaluated the functional significance based on patient-derived xenograft models and analyzed translation alterations by nascent proteomics and ribosome profiling to dissect the role of dynamic rRNA modifications in the control of tumor cellular hierarchy and leukemic stem cell activity. These analyses demonstrate that enhanced 2'-O-Me on ribosomes exterior sites drives AML stem cell phenotypes via preferential translation of amino acid transporter mRNAs in a codon-dependent manner.

Results

A dynamic rRNA ribomethylome in human AML

As one of the key steps in ribosome biogenesis, rRNA is post-transcriptionally modified with 2'-O-methylation by the methyltransferase fibrillarin (FBL). FBL is guided by C/D box snoRNAs for site specificity. In our previously generated LSC proteome dataset, we observed an overrepresentation of FBL and other C/D box snoRNP members in LSC fractions(30) (Supplementary Figure S1A). Transcriptome analysis in 90 primary AMLs indicated that FBL positively correlated with leukemia stem cell (LSC) genes (Supplementary Figure S1B and C) and negatively correlated

with hematopoietic differentiation programs (Supplementary Figure S1D). These findings hinted at a potential association between FBL-induced rRNA 2'-O-Me and AML stem cell phenotypes. Thus, we systematically explored the entire rRNA 2'-O-Me (ribomethylome) for 94 AML specimens as well as for human $CD34^+$ cord blood cells, peripheral blood B cells, T cells, monocytes and granulocytes by performing RiboMethSeq(31). In total, 111 sites (69 sites on 28S, 40 on 18S and 2 on 5.8S rRNA) were found to be 2'-O-methylated in AML blasts and in normal hematopoietic cells (Supplementary table S1). In healthy cells, the extent of 2'-O-Me of each modification site was rather static, with small fluctuation across the entire rRNA sequence (Supplementary Figure S1E and F). Yet, the overall 2'-O-Me pattern clearly separated each cell type from the others, indicating cell type specific ribomethylomes (Fig. 1A). The 2'-O-Me patterns in AML blasts showed far higher levels of heterogeneity (Fig. 1B). In AML patients, only 44 of 111 modification sites were constantly fully methylated (static sites, methylation score > 0.98, variability in methylation score < 0.02), and the other sites exhibited substoichiometric and dynamic methylation (Fig. 1C).

Variation of 2′-O-Me in AML occurred at a subset of apparently coregulated sites. By unsupervised hierarchical clustering based on Pearson's correlation of 2'-O-Me, dynamic sites were categorized into four clusters (Dynamic Methylation Clusters, DyMeC 1 to 4, Fig. 1D and Supplementary table S2). Of note, methylation status on DyMeC 2 correlated with AML developmental stage. Most patients with high 2'-O-Me on DyMeC 2 (55%, 23 of 42 cases) were diagnosed as AML without maturation (FAB M0 and M1). This phenotype occurred only in 16% (6 of 44 cases) of patients with low 2'-O-Me (P = 5.52E-05) (Fig. 1E). Further, patients with high 2'-O-Me showed higher $CD34^+$ blast counts in bone marrow and blood (Supplementary Figure S2A). There was no association between 2'-O-Me and patient's age, gender, bone marrow blast (BMB) percentage, AML type, cytogenetics or mutational profile (NPM1, FLT and CEBPA) (Supplementary Figure S2A). Transcriptome analysis indicated that patients with high rRNA methylation on DyMeC 2 were enriched for leukemia stem cell signatures and depleted for hematopoietic differentiation programs (Fig. 1F and Supplementary Figure S2B). Enrichment of LSC signatures in samples with higher 2'-O-Me on DyMeC 2 was confirmed in a second, independent patient cohort (n = 18, Supplementary Figure S2C and D). This association was specific for DyMeC 2 and did not occur for the other DyMeC clusters (Supplementary Figure S2E to G).

We confirmed the rRNA 2'-O-Me patterns in functionally validated leukemia stem cells and the matched non-LSC counterparts from 5 AML patient(30,32) (Supplementary Figure S3A to C). Nine rRNA sites showed significantly increased 2'-O-Me modification in LSCs (Fig. 1G). All LSC sites were attributed to DyMeC 2 with the exception for 28S C2527 and G4937 (Fig. 1D and G). Of note, no guide snoRNAs are assigned to 28S C2527 and G4937, suggesting that the two sites might be introduced by distinct mechanisms independent of C/D box snoRNPs(18).

On the three-dimensional (3D) ribosome model(33), the static sites mainly located within and surrounding catalytic centers, represented by Gm4166 in the P-tRNA CCA binding pocket, Gm4340 in the E-tRNA binding site, and Um4468 and Gm4469 in the peptidyl transferase center (PTC) (Fig. 1H and Supplementary table S3). In contrast, the DyMeC 2 cluster, including the LSC-associated sites, was mainly located on the ribosome surface distant from catalytic regions (Fig. 1I and Supplementary Figure S3D), suggestive of a 'specialized' function in protein translation control.

The ribomethylome regulates human AML stemness

Given the close association of 2'-O-Me, especially that on DyMeC 2, with immature AML phenotypes and LSC gene expression signature, we hypothesized that 2'-O-Me might represent a novel AML stemness regulator. Knockdown of 2'-O-methyltransferase FBL predominantly reduced 2'-O-Me on cluster DyMeC 2, especially on the LSC sites 18S G1447, 28S G2863, G4560, G4588 and G3723 (Fig. 2A and Supplementary Figure S4A and B). The four static sites in the conserved catalytic centers (28S G4166, G4340, U4468 and G4469) were not affected (Supplementary Figure S4A and C). Decreased FBL expression inhibited colony formation of functionally validated $CD34^{+}CD38^{-}$ leukemic stem cells (Fig. 2B). Next, we aimed to evaluate the relevance of FBL enzymatic activity for leukemogenic functions. Structural analysis of human FBL protein(34) revealed that the amino acids T172, D191, F192, D216 and D236 form a "pocking" domain (Fig. 2C). These sites are predicted to be responsible for substrate binding. We replaced the respective amino acids with alanine to create enzymatically compromised FBL mutants, including mutant $FBL^{T172A,\ D191A,\ F192A}$ (referred as FBL^{Tri}) and $FBL^{T172A,\ D191A,\ F192A,\ D216A}$ (referred as FBL^{Qua}). Doxycycline induced target specific shRNA achieved an 80% reduction in endogenous FBL protein levels in Kasumi-1 leukemia cells (Fig. 2D). Expression of either wildtype or mutated FBL reinstated total FBL protein levels back to 90% of control (Fig. 2D). The ribomethylome was faithfully re-established by wildtype but none of the mutant FBL (Fig. 2E and Supplementary Figure S4D). Functionally, only wildtype FBL rescued AML cell colony formation and proliferation (Fig. 2F and Supplementary Figure S4E).

Engraftment and initiation of human leukemia in immunocompromised mice is the *bona fide* definition of human LSCs. Thus, we expressed either wildtype FBL or FBL^{Qua} mutant in AML patient-derived xenograft (PDX) cells with low leukemogenicity as indicated by long latency. After transplantation into $NOD.Prkdc^{scid}.Il2rg^{null}$ (NSG) mice, leukemia burden was repetitively monitored by bioluminescence imaging. Wildtype FBL accelerated leukemogenesis, whereas the enzymatically inactive FBL^{Qua} mutant failed to do so (Fig. 2G and H). We further observed an increase in the fraction of leukemia stem cells (represented by $GPR56^{+}CD34^{+}$ cells) in PDX cells overexpressing wildtype FBL (Supplementary Figure S5A and B). FBL^{WT} PDX cells formed more colonies upon plating in methylcellulose (Supplementary Figure S5C). We determined LSC frequencies in these PDX cells by *in vivo* limiting dilution analysis. FBL^{WT} PDX cells showed nearly

215 a 5-fold and 10-fold increase in LSC frequency compared to empty control and
216 FBL^{Qua} PDX cells, respectively (1 in 4,187 vs. 1 in 20,646, P = 0.0189, and vs. 1 in
217 43,309, P = 0.0006) (Fig. 2I and Supplementary Figure S5D). Forced expression of
218 FBL promoted engraftment of primary AML blast (Supplementary Figure S5E),
219 which functionally confirmed FBL induced LSC phenotype. Moreover, FBL
220 expression transformed non-LSC leukemia cells into functional engrafting LSCs in
221 primary and PDX AML samples. Upon expression of empty vector, the $CD34^+CD38^+$
222 populations from two specimens showed very poor engraftment in only 1 of 11 mice
223 (1/7 and 0/4 respectively). Upon enforced FBL expression in these $CD34^+CD38^+$ cells,
224 7 out of 8 mice could be engrafted (5/5 and 2/3 respectively; P = 0.0012, Fisher's
225 exact test) (Supplementary Figure S5F and G). Taken together, these data
226 demonstrated that an FBL-induced ribomethylome induced an LSC phenotype and
227 accelerated leukemia progression.
228
229 **The dynamic ribomethylome regulates translation of amino acid transporters**
230 The dynamic ribomethylome might function by redirecting protein translation. We
231 performed nascent proteomics to evaluate active protein synthesis using pulsed
232 azidohomoalanine (pAHA) labeling in combination with pulsed SILAC
233 (pSILAC)(35). Proteins newly synthesized within a six-hour time window were
234 captured from FBL knockdown or control cells (Supplementary Figure S6A and B),
235 and their abundance was normalized to read density of transcripts identified by
236 mRNA-seq (Supplementary Figure S6C). This approach enabled us to define genes
237 which were differentially regulated at the translation level. FBL knockdown did
238 neither affect the total ribosome level (Supplementary Figure S6D to F) nor global
239 protein translation (Fig. 3A). We obtained a set of 213 proteins with suppressed
240 translation upon decreased FBL levels (Fig. 3A and Supplementary table S4). The
241 downregulated proteins were enriched for six pathways, with mTORC1 signaling on
242 the top (Fig. 3B). The upregulated proteins were mainly enriched for immune cell
243 development (Supplementary Figure S6G). The mTORC1 pathway acts as a hub to
244 coordinate protein translation and metabolic demand with the switch of stem cell fate
245 from self-renewal to differentiation(3). Among mTORC1 pathway genes, synthesis of
246 all amino acid transporter proteins captured in our assay was decreased upon
247 suppression of rRNA 2'-O-Me (Fig. 3C). In line, metabolic screening by Gas
248 Chromatography/Mass Spectrometry revealed that amino acids were the metabolites
249 most strongly affected by FBL knockdown (Supplementary Figure S6H). A targeted
250 metabolite analysis showed that multiple amino acids, especially glutamine, glutamic
251 acid, alanine and proline were significantly reduced in FBL knockdown cells
252 (Supplementary Figure S6I). Amino acid metabolism-related glutathione and α-
253 ketoglutarate were also significantly reduced in knockdown cells (Supplementary
254 Figure S6J and K). Vice versa, overexpression of FBL in PDX cells *in vivo* increased
255 the amino acid transporter proteins SLC1A5, SLC2A1, SLC7A5, SLC38A1 and
256 SLC38A10 even though the mRNA levels remained unchanged (Fig. 3D and
257 Supplementary Figure S6L). Consistent with this, we observed increased intracellular
258 levels of glutamine, glutamic acid, glycine, aspartic acid and histidine in these AML

PDX cells (Fig. 3E). Altered amino acid metabolism has been reported as a hallmark feature of leukemic stem cells(36,37). These data suggested that enhanced amino acid metabolism is an important functional consequence of increased 2′-O-Me in leukemic stem cells.

Next, we performed ribosome profiling to investigate the interaction of ribosomes with amino acid transporter mRNAs under different rRNA 2'-O-Me conditions (Supplementary Figure S7A to C). Indeed, FBL knockdown altered codon usage (Fig. 3F and Supplementary Figure S7D and E). Increased ribosome occupancy was found at in-frame P-site at the start ATG codon, codons for Alanine (GCC, GCG, GCT), Cysteine (TGC), Glycine (GGC), Isoleucine (ATC, ATT), Leucine (CTG, CTA, CTT), Proline (CCA), Arginine (AGA, CGG), Threonine (ACC), Valine (GTA, GTG) and Tryptophan (TGG) (Fig. 3F and Supplementary Figure S7F), indicating decelerated translation elongation at these codons. Notably, most of these codons belong to optimal codons which are supposed to increase mRNA stability and translation efficiency(38-40) (Supplementary Figure S7G). Codon optimality coordinates the expression of functionally related genes, i.e., important enzymes involved in glycolysis(41,42). We analyzed the codon content of amino acid transporter genes. Optimal codons were over-represented in amino acid transporters, especially in transporters downregulated by 2'-O-Me suppression (Fig. 3G). In line, we observed increased ribosome pausing specifically on amino acid transporter mRNAs (Supplementary Figure S7H and I), consistent with the reduced translation rate. Of note, optimal codons were neither enriched in other genes such as the mTOCR1 pathway, nor in genes involved in glycolysis shown to be supressed by FBL knockdown (Supplementary Figure S7J and K). Translational downregulation of such genes might be an *in-trans* effect of ribosome pausing on the highly expressed amino acid transporters (up to about 20% of Actin mRNA, Supplementary Figure S6L), due to the shared tRNA and translation apparatus(43). Further, we did not observe reduced mTOCR1 activity after FBL knockdown, as phosphorylation of p70S6 kinase on Thr389 and 4E-BP1 on Thr37/46, the direct downstream targets of mTORC1, was not altered (Supplementary Figure S7L). Together, these data suggest that FBL induced rRNA methylation regulates LSC mainly through optimizing the translation of specific amino acid transporters by affecting optimal codon usage, even though FBL may have additional functions.

Methylation of 18S G1447 (Gm1447) determines LSC activity

Beyond global rRNA methylation patterns, single site modification might impact on leukemia stem cell activity. We focused on 18S G1447, a LSC site in DyMeC 2 which locates on the surface of the small subunit of the human ribosome (Supplementary Figure S8A). Gm1447 was increased in human LSCs compared to non-LSC counterparts in primary AMLs (Fig. 4A). Gm1447 varied substantially (methylation score ranging from 0.54 to 0.95) across primary AML blasts, whereas the upstream modification site U1442 was constitutively fully methylated (Fig. 4B). Comparing the transcriptomes of $Gm1447^{high}$ AMLs with $Gm1447^{low}$ samples

revealed a positive enrichment for LSC genes and negative enrichment for hematopoietic differentiation genes in two independent patient cohorts (Fig. 4C and Supplementary Figure S8B and C). These findings suggested an association of Gm1447 with AML stemness.

The guiding snoRNA for Gm1447 is SNORD127 (Supplementary Figure S8D) which is expressed from intron 10 of gene *PRPF39* on chromosome 14(44,45). To suppress Gm1447, we generated SNORD127 knockout in the AML cell lines OCI-AML2 and Kasumi-1 using CRISPR/Cas9 coupled with paired gRNAs flanking SNORD127 sequence (Supplementary Figure S8E). Of note, no homozygous deletion clone was obtained from 200 screened single clones, which indicated that SNORD127 might be essential at least in leukemic cells. SNORD127 monoallelic deletion (SNORD127$^{+/-}$) caused an about 60% decrease in SNORD127 levels and in Gm1447 (Fig. 4D and Supplementary Figure S8F). The loss did not affect other sites and had no effect on host gene expression (Fig. 4D and Supplementary Figure S8G). To confirm the decrease in Gm1447, we performed cryo-EM single particle analysis for 80S ribosome purified from SNORD127$^{+/+}$ and SNORD127$^{+/-}$ Kasumi-1 cells. We obtained the 80S ribosome structures with high resolution of 2.5 Å and 2.7 Å on average, respectively. Although the 40S head part, where the G1447 locates, displayed decreased local resolution due to its dynamic movement, it was sufficient to identify and compare the 2′-O-Me modification of the rRNA nucleotides. Clearly, the corresponding density bump of the 2′-O-Me modification on G1447 presented in ribosomes in wildtype cells became much weaker in SNORD127$^{+/-}$ cells (Fig. 4E). This finding confirmed decreased 2′-O-Me upon heterozygous SNORD127 deletion. Loss of modification on G1447 did not alter local peptide chain conformation. However, decreased G1448 methylation altered the ribosome interactome. We observed nucleolar protein LYAR on the decoding center of the 40S ribosomal subunit in SNORD127$^{+/+}$ but not in the SNORD127$^{+/-}$ cells (Fig. 4E). Loss of LYAR-ribosome association in SNORD127$^{+/-}$ cells was confirmed by sucrose density gradient ribosome fractionation and Western Blot analysis (Supplementary Figure S8H). Of note, LYAR has been implicated in maintenance of pre-rRNA processing and mouse embryonic stem cell self-renewal(46,47).

We identified proteins that were differentially translated upon Gm1447 repression. Only 12 genes were found less translated by more than 2-fold in nascent proteomics analyses (Fig. 4F). The SLC38A10 amino acid transporter ranked among the most repressed proteins (Fig. 4F). SLC38A10 mRNA levels were not affected (Supplementary Figure S8I). Accordingly, SNORD127$^{+/-}$ cells showed reduced intra-cellular glutamine, glutamic acid, glycine and aspartic acid levels (Supplementary Figure S8J). Functionally, the SNORD127 heterozygous deletion reduced clonogenic capacity of AML cells (Supplementary Figure S9A and B). Lentiviral delivery of SNORD127 in SNORD127$^{+/-}$ cells specifically restored Gm1447 (Supplementary Figure S9C) and rescued the clonogenic growth defect (Supplementary Figure S9D). The clonogenic defect was also partially rescued by wildtype but not mutant FBL

(Supplementary Figure S9E), demonstrating the functional importance of Gm1447 for leukemia cells. In *in vivo* transplantation assays, SNORD127 heterozygous deletion reduced leukemic engraftment (Fig. 4G and Supplementary Figure S9F) and prolonged the survival of recipient animals (median survival 39 vs. 49 days, P = 0.0002) (Fig. 4H). Conversely, enforced expression of SNORD127 in two AML cell lines and three human primary AML cells promoted leukemic engraftment (Fig. 4I to K, Supplementary Figure S9G and H). The enhanced engraftment was in line with the increased leukemia stem cell pool ($CD34^{+}CD38^{-}$) in primary AML cells transduced with SNORD127 (Supplementary Figure S9I and J). Finally, the increased LSC frequency upon SNORD127 overexpression was confirmed by *in vivo* limiting dilution transplantation (1 in 1537 vs. 1 in 19317, P = 0.0015) (Fig. 4L and Supplementary Figure S9K).

Discussion

Our study unveils a critical role for dynamic rRNA 2'-O-Me in governing protein translation and cancer stem cell phenotypes. Recent studies illustrated distinct 2'-O-Me changes on rRNA sites in multiple cellular models and tissues(27,28,31), highlighting them as a potential source of ribosome diversity for gene expression regulation. But, the mechanisms and the functional outcome remain to be discovered. Here, through profiling rRNA 2'-O-Me in primary AML samples, we show that leukemia stem cell-enriched FBL and its mediated rRNA 2'-O-Me modulate protein translation, impact leukemia stem cell phenotypes and contribute to their propagation.

We established the ribomethylome landscape in human AML and normal hematopoietic cells. This revealed dynamic and cell type specific rRNA 2'-O-Me patterns. These modification patterns provide an additional layer for ribosome diversity, which, in turn, may confer a strategy to enable cells to co-opt their transcription profile and translation machineries for the formation of cell type specific proteome. In AMLs, the dynamic methylation mainly affects ribosome exterior sites, but not evolutionarily conserved sites. Our findings complement the conception that a core set of evolutionarily conserved modification render the ribosome capable of efficient and accurate translation, while the evolutionarily extended modifications might confer regulatory functions to ribosome(16).

Importantly, we find that leukemia stem cells can exploit this regulatory circuit to maintain enhanced self-renewal, providing novel insights into this poorly understood mechanism. FBL and its mediated rRNA 2'-O-Me, as demonstrated by Gm1447, are exquisitely regulated in primary AMLs, with close association with leukemia stem cell gene expression signature and phenotype. This is consistent with findings that the tight control in ribosome biogenesis and protein synthesis are essential to establish and maintain cell identity and function. Accordingly, our study indicates that FBL and rRNA 2'-O-Me preferentially regulate the translation of genes crucial for leukemia stem cells. Thus, rRNA 2'-O-Me may present one of the major epitranscriptomic programs that governs protein synthesis to confer AML stemness phenotypes. Of note,

the LSCs used for rRNA 2'-O-Me characterization in this study were derived from the $CD34^+CD38^-$ population. However, since FBL protein abundance was also increased in $CD34^+CD38^+$ LSCs(32), it appears that FBL mediated rRNA 2'-O-Me represents a regulator of LSCs, regardless of their immunophenotype. In addition, the rRNA 2'-O-methyltransferase FBL shows high baseline expression in mouse embryonic stem cells and is required for the maintenance of pluripotency(48). Pan-cancer analysis indicates upregulation of FBL in multiple types of cancer (Supplementary Figure S9L). Heterogeneity in rRNA 2'-O-Me has also recently been observed in diffuse large B-cell lymphoma and breast cancer(27,28). Hence, the FBL-mediated dynamic ribomethylome mediated stemness regulation, similar to those we identify within the context of AML, may therefore extend to other tumor entities including solid cancer.

A metabolic feature for leukemia stem cell is their dependence on elevated amino acid uptake and metabolism for oxidative phosphorylation and survival(36). How leukemia stem cells selectively activate proteins involved in amino acid metabolism is not immediately apparent, since cancer stem cells are characterized by low global protein translation rates(3,6,7). Previous studies showed that selective translation could be steered in stem cells by specific translation initiation factors, mRNA splicing and ribosome levels(12,49-51). More recent studies further highlight the importance of dynamic changes in RNA modifications in rewiring the genetic information decoding in stem cells(52). Our study indicates that, through increased 2'-O-Me, LSCs are able to enhance the translation of essential amino acid transporters without changes on mRNA level to meet metabolic requirements. mRNA features in 5' untranslated region (UTR), upstream open reading frames (uORFs) and 3' UTR also provide important regulatory elements for translation control during stem cell self-renew and differentiation(12,53,54). We demonstrate that the codon composition of mRNA mediates the selective translation conferred by dynamic rRNA 2'-O-Me. The higher content of optimal codons in amino acid transporter genes confers an advantage to their translation promoted by rRNA 2'-O-Me modification.

Taken together, this study reveals a novel regulatory pathway in cancer pathogenesis. Epitranscriptomic modifications drive cancer stem cell phenotypes by a molecular strategy that integrates dynamic ribosome methylation, selective protein translation and cellular metabolism.

Methods:

Plasmid construction and cell culture. Human Fibrillarin (FBL) cDNA were purchased from Source BioScience (Clone ID: 3504198). Point mutations of FBL were introduced by custom-designed mutant primers. C-terminal V5 epitope-tagged wildtype and mutant FBL were cloned into lentivirus expression vector PCDH-EF1α-T2A-eGFP between EcoRI/BamHI. ShRNAs were cloned into pLKO.1 vector with GFP as the selection marker, or Doxycycline inducible Tet-pLKO-puro vector (Cat. 21915, Addgene). Targeting sequences of shRNA are GAT TTC GGA AGG AGA TGA CAA for shFBL#2, GCT GTC AGG ATT GCG AGA GAT for shFBL#4, and

435 CGC TGA GTA CTT CGA AAT GTC for shCtrl. For SNORD127 overexpression,
436 cDNA of SNORD127 was amplified from genomic DNA of HEK293 cells and was
437 first inserted into pLKO.1-GFP vector between AgeI/EcoRI under U6 promoter. Then
438 SNORD127 sequence together with the upstream U6 promoter were subcloned into
439 PCDH-EF1α-eGFP vector in ClaI site with In-Fusion kit (Cat. 638909, Takara).
440
441 Lentiviral vector encoding a doxycycline inducible Cas9 was purchased from
442 Addgene (Lenti-iCas9-neo, Cat. 85400). Paired sgRNAs for SNORD127 deletion
443 were cloned into pDECKO-mCherry vector (Cat. 78534, Addgene) by In-Fusion
444 cloning. In pDECKO vector, sgRNA1 (GTG GTC AGT GTA TTT TCA CTG) is
445 driven by the U6 promoter and sgRNA2 (CTG ATT ACT AAG TAG AAC AG) is
446 driven by H1 promoter.
447
448 Cell lines were cultivated at 37 °C in a humidified incubator with 5% CO_2 (Thermo
449 Scientific). 293T cells were cultured in Iscove's modified Dulbecco's medium (IMDM)
450 (Cat. 12440061, Thermo Scientific) supplemented with 10% FBS (Cat.S0165,
451 BIOCHROM) and 1% penicillin–streptomycin (Sigma). Human leukemia cell lines
452 were cultured in RPMI1640 medium (Cat. R8758, Sigma) with 20% FBS (Kasumi-1
453 cells) or 10% FBS (OCI-AML2 and HL60 cells), supplemented with 1% penicillin–
454 streptomycin. For cells transduced with Tet (tetracycline)-inducible vectors,
455 doxycycline-free serum (Cat. 631105, Clontech) was used. The cell lines have been
456 authenticated and tested for mycoplasma contamination.
457
458 **Human primary samples.** AML samples for RiboMethSeq and RNA-Seq were
459 collected from diagnostic bone marrow aspirations at University Hospital Dresden,
460 Germany. The 5 AML samples with determined engrafting capacity for each
461 CD34/CD38 population have been described previously(30,32). Cord blood samples
462 from normal deliveries were collected from the University Hospital in Heidelberg.
463 Stem and progenitor cells were enriched by positive selection using CD34 UltraPure
464 MicroBead (Cat. 130-100-453, Miltenyi Biotec) according to manufacturer's
465 instructions. Peripheral blood samples from healthy donors were obtained from blood
466 bank Heidelberg. Monocyte, Granulocyte, B-cell and T-cell were isolated from
467 peripheral blood with CD19 MicroBead, CD66abce MicroBead, CD19 MicroBead
468 and CD3 MicroBead (Miltenyi Biotec). Total RNA was isolated from the primary
469 cells with miRNeasy Mini Kit (Cat. 217004, Qiagen). For sample collection, the
470 'written informed consent' were obtained from all the patients. All experiments
471 involving human samples were conducted in compliance with the Declaration of
472 Helsinki and all relevant ethical regulations were approved by the ethics committees
473 of the medical faculties of the universities in Heidelberg and Dresden.

474 **Lentivirus production and human leukemia cell infection.** pLKO.1 (for
475 constitutive FBL knockdown), Tet-pLKO-puro (for inducible FBL knockdown),
476 PCDH vector (for FBL expression), Lenti-iCas9-neo (for inducible Cas9 expression)
477 or pDECKO-mCherry (for paired sgRNA delivery) together either with the secondary

generation packaging vectors (pPLP1, pPLP2 and VSV-G), or with the third generation packaging system (pRSV-Rev, pMDLg/pRRE, pMD2.G for PDX cells)(55) were transfected into 293T cell with Turbofect reagent (Thermo Scientific). Medium containing lentivirus particles was collected at 72 h after transfection and lentivirus particles were precipitated by centrifugation at 29,000 g at 4 °C for 2 hours. Transductions were conducted by the incubation of virus and cells in the presence of 8 µg ml^{-1} Polybrene (Cat. TR-1003-G, Millipore).

Mouse experiments. NOD.*Prkdc*^{scid}.*Il2rg*^{null} (NSG) mice were bred and housed under specific pathogen-free conditions in the central animal facility of the Helmholtz Center Munich and of the German Cancer Research Center (DKFZ). Animal experiments were approved and performed in accordance with all regulatory guidelines of the official committee (Regierung von Oberbayern and Regierung von Regierungspräsidium Karlsruhe). No statistical methods were used to estimate sample size.

Generation of AML PDX models: generation of firefly luciferase expressing AML491 PDX cells was performed as previously described(55,56). AML491, AML03, AML08, AML661 and AML494 cells were lentivirally transduced to express FBL wildtype, FBL mutant, SNORD127 or empty vectors. Transduced cells were enriched using flow cytometry by gating on GFP expression as previously described(57). For AML491 and AML08, the LSC $CD34^{+}CD38^{-}$ and non-LSC $CD34^{+}CD38^{+}$ populations were further sorted. Then, sorted AML cells were injected into the tail vein of 10- to 12-week-old NSG mice after irradiation with a dose of 1.75 Gy. The *in vivo* engrafting experiments of human cell lines, including $SNORD127^{+/+}$ and $SNORD127^{+/-}$ OCI-AML2 and Kasumi-1 cells, HL60 cells and OCI-AML2 cells expressing empty vector or SNORD127 were performed with same procedure as described above.

Assessment of Leukemic Engraftment: Starting at day 14 after transplantation, tumour burden was regularly assessed using IVIS Lumina II (Caliper) with Living Image version 4.3.1 software (PerkinElmer) for firefly luciferase expressing AML491 PDX model. For the other PDX models, 50µl blood was repetitively collected by tail vein or bone marrow aspiration was performed. Blood samples and bone marrow aspirates were analyzed by flow cytometry after staining for human CD45 and human CD33 as previously described(55). At advanced leukemic disease, mice were sacrificed by exposure to CO_2 or cervical dislocation and PDX cells were re-isolated from murine bone marrow for further analyses. In addition, daily monitoring of mice for symptoms of disease (ruffled coat, hunched back, weakness, and reduced mobility) determined the time of sacrificing for injected animals with signs of distress.

In vivo limiting dilution transplantation assay (LDTA): PDX cells expressing empty vector, wildtype or mutant FBL and DPX cells expressing empty vector or SNORD127 were FACS-sorted from the bone marrow of corresponding animals. To avoid bias from animals, PDX cells from two mice of each group were mixed for

522 LDTA. Female NSG mice at the age of 12 weeks were irradiated with 1.75 Gy one
523 day before transplantation. Cells were injected into groups of mice at different dose
524 each animal. Each group contained 4 to 5 mice. Engraftment was assessed 10 weeks
525 after transplantation and a threshold of 0.1% human PDX cells in bone marrow was
526 used as positive for engraftment.
527
528 **FBL Rescue experiments.** Rescue of FBL knockdown with wildtype and mutant
529 FBL was performed in Kasumi-1 cells. Kasumi-1 cells were first infected with
530 lentivirus expressing doxycycline inducible shCtrl and shFBL#4 (targeting 3'-UTR of
531 endogenous FBL mRNA). The infected cells were then selected in medium with 2
532 ug/ml puromycin for 10 days. The established inducible knockdown cells were further
533 used for FBL rescue experiments. The empty vector, wildtype or mutant FBL were
534 delivered to inducible FBL knockdown cells by lentivirus infection. FBL knockdown
535 was induced with 100 ng ml^{-1} doxycycline for three days.

536 **Colony formation assay**. For AML LSC populations, cells were transduced with
537 lentivirus expressing shFBL#2, #4 or shCtrl. Forty-eight hours after transduction,
538 GFP^+ cells were FACS-sorted into methylcellulose medium MethoCult™ H4034
539 (StemCell Technologies) for culture. For AML PDX cells, $mCherry^+$ PDX cells were
540 FACS-sorted from bone marrow of NSG recipient mice into MethoCult™ H4034
541 (StemCell Technologies). Each culture contained 20,000 cells in 0.5 ml
542 methylcellulose medium. For Kasumi-1 and OCI-AML2 derived cells, MethoCult™
543 H4230 methylcellulose medium (StemCell Technologies) was used according to the
544 manufacturer's instructions. Each culture contained 300 Kasumi-1 cells or 800 OCI-
545 AML2 cells in 0.5 ml of methylcellulose medium in 12-well plate. Colonies formed
546 by AML LSCs and leukemia cell lines were evaluated and scored after 14 days in
547 culture, and colonies formed by PDX cells were scanned after 20 days in culture.

548 **Western blot analysis.** Cells were washed two times with ice-cold PBS and lysed in
549 RIPA buffer (Cat. 89900, Thermo Scientific) with proteinase inhibitor cocktail (Cat.
550 11873580001, Roche). After incubation on ice for10 min, cell lysates were
551 centrifuged at 12,000 g for 10 min. Supernatants were collected and heated at 70°C
552 for 10 min after adding NuPAGE™ LDS Sample Buffer (Cat. NP0007, Thermo
553 Scientific). Protein lysates were resolved on NuPAGE™ 4 to 12% Bis-Tris gels (Cat.
554 NP0321BOX, Thermo Scientific) with NuPAGE™ MES SDS running buffer (Cat.
555 NP0002, Thermo Scientific) and blotted on Amersham™ Protran® Western blotting
556 membranes, nitrocellulose (Cat. GE10600001, Sigma). Membranes were blocked
557 overnight at 4 °C in PBS containing 0.5% (v/v) Tween-20 with 5% milk powder.
558 Primary antibodies against anti-Fibrillarin (Cat. ab5821, Abcam), anti-V5 tag (Cat.
559 ab9116, Abcam), anti-beta Actin (Cat. ab6276, Abcam), anti-PRPF39 (Cat.
560 GTX104949, Genetex), anti-SLC38A10 (Cat. ab121830, Abcam), anti-
561 LAT1/SLC7A5 (Cat. 5347S, Cell Signaling), anti-ASCT2/SLC1A5 (Cat. 8057S, Cell
562 Signaling), anti-Glut1/SLC2A1 (Cat. 12939S, Cell Signaling), anti-
563 SNAT17SLC38A1 (Cat. 36057S, Cell Signaling), anti-LYAR (Cat. ab182138,

564 Abcam), anti-RPL23A (Cat. Ab157110, Abcam), anti-4E-BP1 (Cat. 9644T, Cell
565 Signaling), anti-Phospho-4E-BP1(Thr37/46) (Cat. 2588T, Cell Signaling), anti-p70
566 S6 Kinase (Cat. 2708T, Cell Signaling), anti-Phospho-p70 S6 Kinase (Thr389) (Cat.
567 9234T, Cell Signaling) were incubated 2 hours at room temperature in blocking
568 solution. Secondary antibodies (horseradish peroxidase-linked anti-rabbit-IgG or anti-
569 mouse-IgG antibody, Dianova) were incubated for 90 min at room temperature in
570 blocking solution. Immunocomplexes were detected using an ECL^{TM} Prime reagent
571 (Cat. RPN2232, GE Healthcare) and acquired with Amersham Imager 600 system
572 (GE Healthcare).

573 **Quantitative RT-PCR.** The total RNA was extracted with miRNeasy Mini Kit
574 (Qiagen) combined with RNase-Free DNase (Qiagen) treatment according to the
575 manufacturer's instructions. cDNA of mRNA was synthesized using a SuperScript™
576 IV Reverse Transcriptase (Cat. 18090050, Thermo Scientific) according to the
577 manufacturer's protocol. Real time-PCR was performed on CFX96 Touch System
578 (BioRad) using ssoAdvanced Universal SYBR Green SuperMix (Cat. 1725272,
579 BioRad). The following primers were used: SLC7A5 (forward: 5′ - GTG TAC GTG
580 CTG ACC AAC CT; reverse: 5′ - TGA CGC CCA GGT GAT AGT TC), SLC1A5
581 (forward: 5′ - TTA CTC TTT GCC CGC CTT GG ; reverse: 5′ - TAG GGG TTT
582 TTG CGG GTG AA), SLC2A1 (forward: 5′ - CTG GCA TCA ACG CTG TCT TC;
583 reverse: 5′ - AAC AGC GAC ACG ACA GTG AA), SLC38A1 (forward: 5′ - TCC
584 CTG CAT TGT TCC AGA GC; reverse: 5′ - TGA CGG GTG GCA AAC AAA TG),
585 SLC1A5 (forward: 5′ - CTC GAG ACT CCA AGG GGC T; reverse: 5′ - CCG GGA
586 ACC GCA GTA GC), Actin (forward: 5′ - ACA GAG CCT CGC CTT TGC; reverse:
587 5′ - CGC GGC GAT ATC ATC ATC CA), GAPDH (forward: 5′ - ACT GCC AAC
588 GTG TCA GTG G; reverse: 5′ - CAC CCT GTT GCT GTA GCC A).

589 cDNA for snoRNA were synthesized with Mir-X miRNA First-Strand Synthesis Kit
590 (Cat. 638313, Clontech). SnoRNAs were detected with gene-specific forward primer
591 and universal reverse primer. The forward primer for SNORD127 is 5′ - GGC AAC
592 TGT GAT GAA AGA TTT GGT.

593 **Flow cytometry.** Leukemia stem cell and non-leukemia stem cell fractions were
594 FACS-sorted from primary AML samples. Frozen vials of AML samples were thawed
595 in 37°C water bath in IMDM medium with 10% FBS, 100 µg ml^{-1} DNase I (Sigma).
596 After filtering through the 40 µm cell strainer, cells were stained with the following
597 antibodies: Alexa Fluor® 488 anti-human CD34 (Cat. 343518, Biolegend), PE anti-
598 human CD38 antibody (Cat. 303506, Biolegend), and a lineage cocktail consisting of
599 CD4-APC (Cat. 300514, Biolegend), APC anti-human CD20 (Cat. 302310,
600 Biolegend), APC anti-human CD8a (Cat. 301014, Biolegend), APC anti-human CD19
601 (Cat. 302212, Biolegend). Before sorting, 1 µl of 10 mg ml^{-1} DAPI (Cat. 422801,
602 Biolegend) was added to the cell suspension. Cells were sorted into four quadrants
603 according to CD34 and CD38 expression within the DAPI negative and lineage-
604 negative gate.

605 To check the purity of isolated healthy hematopoietic cells, the following antibodies
606 were used: CD34-BV421 (Cat. 562577, BD Biosciences), CD14-PE (Cat. 301850,
607 Biolegend), CD15-PE-Cy7 (Cat. 560827, BD Biosciences), CD3-BV421 (Cat.
608 300434, Biolegend), CD19-PE-Cy7 (Cat.302216, Biolegend).

609 For PDX cells, total bone marrow of NSG recipient mice were stained with APC anti-
610 human CD34 (Cat. 340441, BD) and PE anti-human GPR56 (Cat. 358203, Biolegend).
611 Before flow cytometry analysis, 1 µl of DAPI (10 µg ml^{-1}) was added to the cell
612 suspension to gate out the dead cells.

613 **RiboMethSeq.** RiboMethSeq was performed as previously described with minor
614 modifications(31). Briefly, 100 ng total RNA was hydrolyzed in alkaline buffer (50
615 mM bicarbonate, pH 9.2) at 95 °C for 12 min to achieve an average fragment size of
616 about 30 nucleotides. The rRNA fragment was purified by ethanol precipitation using
617 3 M Na-OAc pH 5.2 and glycogen as a carrier. RNA fragments were proceeded to
618 end repair with 5 U of Antarctic Phosphatase (NEB, UK) for 30 min at 37 °C for 3'-
619 end dephosphorylated. After heat inactivation of the phosphatase, the 5'-end of RNA
620 fragments were phosphorylated using T4 PNK and 1 mM ATP for 1 hour at 37 °C.
621 Libraries were prepared using the NEBNext® Small RNA library prep kit, followed
622 by single end sequencing on Illumina NextSeq500. Reads trimming was performed
623 with cutadapt to remove adapter sequence and reads below 15 nucleotides were
624 discarded. The filtered reads were mapped to rDNA sequences with bowtie2 reference
625 sequence file containing rDNA sequences of U18, U28 and U5.8S. Methylation was
626 calculated by ScoreC as described before(31) based on the reads on 5'-end of
627 fragment. Annotation of modification sites as well as rRNA sequence was
628 downloaded from https://www-snorna.biotoul.fr.

629 **Ribosome profiling library preparation.** Cells were grown in culture medium
630 (RPMI-1640 with 20% FBS) with 100 µg ml^{-1} cycloheximide (CHX, Cat. 4859,
631 Sigma) at 37 °C for 10 min. Cells were collected and washed with PBS (with 100 µg
632 ml^{-1} CHX) twice. Afterwards, cell lysis was performed on ice for 10 min in lysis
633 buffer (20 mM Tris-HCl pH 7.4 (Cat. AM9850G and Cat. AM9855G, Thermo
634 Scientific), 150 mM NaCl (Cat. AM9760G, Thermo Scientific), 5 mM $MgCl_2$ (Cat.
635 AM9530G, Thermo Scientific), 1 mM dithiothreitol (DTT) (Cat. 43816, Sigma), 1%
636 Triton X-100 (Cat. T8787, Sigma), 25 U ml^{-1} of Turbo DNase I (Cat. AM2238,
637 Thermo Fisher Scientific) containing 100 µg ml^{-1} of CHX. Lysates were further
638 sheared by passing through a 26G needles four times. Nuclei and debris were
639 removed by centrifugation at 12,000 g for 10 min, and the RNA concentration of the
640 cell lysate was measured with Qubit kit (Thermo Fisher Scientific). To generate
641 ribosome protected fragments (RPF), 20 µg of total RNA were dilute with polysome
642 buffer (20 mM Tris-Cl pH 7.4, 150 mM NaCl, 5 mM $MgCl_2$, 1 mM DTT, 100 µg ml^{-1}
643 of CHX) to 200 ul, and treated with 7.5 µl of RNase I (100 U $µl^{-1}$, Cat. AM2294,
644 Invitrogen) for 45 min at room temperature with gentle mixing. Digestion was
645 blocked by adding 10 µl of SUPERase·In RNase inhibitor. The reaction was cleaned
646 up with MicroSpin S-400 Columns (Cat. GE27-5140-01, Sigma), followed by

647 purification using RNA Clean & Concentrator-25 kit (Cat. R1017, Zymo Research).
648 The eluted RNA was pelleted by ethanol precipitation. Size selection of RPF with a
649 length of 26–34 nucleotides was performed on 15% polyacrylamide TBE-urea gel
650 (Cat. EC6885BOX, Thermo Fisher Scientific). End repair of RPF was performed with
651 10 U T4 PNK treatment (Cat. M0201S, NEB) at 37 °C for 1 hour. The libraries were
652 prepared with NEBNext® Small RNA Library Prep Set for Illumina®. The library
653 DNA was purified with AMPure beads (Cat. 63881, Beckman Coulter) at the ratio of
654 1.8:1. The library size was measured on Bioanalyzer (Agilent). All samples were
655 multiplexed and sequenced on Illumina NextSeq500.

656 **Ribosome profiling data processing and analysis.** Reads were processed by
657 removing 5' adapters, discarding reads shorter than 20 nucleotides and trimming the
658 first nucleotide of the remaining reads. Reads mapping on human rRNAs (obtained
659 from https://www.ncbi.nlm.nih.gov/nuccore/555853) and tRNAs (obtained from
660 GtRNAdb (http://gtrnadb.ucsc.edu/genomes/eukaryota/Hsapi19/hg19-tRNAs.fa))
661 were removed. The remaining reads were mapped onto the human transcriptome.
662 Antisense and duplicate reads were removed. All alignments were performed with
663 Bowtie 2 (v.2.2.6) using the default settings.

664 Data analysis was performed with riboWaltz R package, RiboToolkit and diricore(58-
665 60). Briefly, BAM files were loaded into the riboWaltz R package. Reads were
666 regarded as duplicates and removed by the function 'duplicates_filter' when they
667 were mapped on the same transcript and shared both the 5' extremity and the 3'
668 extremity. After annotation, the function 'psite offset' was executed to identification
669 of the P-site position within the reads. Then 'region_psite' was used to calculate the
670 percentage of P-sites falling in the three transcript regions (5′ UTR, CDS and 3′ UTR).
671 'rlength_distr' was performed to calculate the distribution of read lengths.
672 'frame_psite' was used to calculate the percentage of P-sites falling in the three
673 possible translation reading frames. The function 'metaprofile_psite' was used to
674 generate the metaprofiles based on the P-site position and to visualize trinucleotide
675 periodicity along coding sequences. After the above quality control steps,
676 'codon_usage_psite' was used to compare the codon usage index between shCtrl and
677 shFBL samples. 'codon_coverage' was used to compute the read footprints or P-sites
678 mapping on each triplet of annotated coding sequences and UTRs. The changes codon
679 usage identified by riboWaltz was further confirmed with RiboToolkit and diricore.
680 To calculate pause score we normalized the read count at each codon of a gene by
681 dividing by the mean read count at all codons for the gene.

682 **RNA-Seq.** A total amount of 1μg RNA per sample was used as input material for the
683 RNA sample preparations. Sequencing libraries were generated using NEBNext®
684 Ultra™ RNA Library Prep Kit for lllumina® (NEB, USA) following manufacturer 's
685 recommendations. The generated libraries were applied to Illumina platform for
686 paired-end sequencing. Raw reads of FASTQ format were firstly processed through
687 fastp. Clean reads were obtained by removing reads containing adapter and poly-N

688 sequences and reads with low quality from raw data. Paired-end clean reads were
689 mapped to the human genome using HISAT2 software. FeatureCounts was used to
690 count the read numbers mapped of each gene, including known and novel genes. Then
691 FPKM (Fragments Per Kilobase of exon per Million mapped fragments) of each gene
692 was calculated based on the length of the gene and reads count mapped to this gene.
693 Differential expression analysis between two conditions/groups was performed using
694 DESeq2 R package. The resulting P values were adjusted using the Benjamini and
695 Hochberg's approach for controlling the False Discovery Rate (FDR). Genes with an
696 adjusted P value < 0.05 found by DESeq2 were assigned as differentially expressed.

697 **Nascent proteomics and data analysis.** Nascent proteomics was performed as
698 previously described(20). The cells were washed twice with Phosphate Buffered
699 Saline (PBS) and cultured in amino acid-depletion medium (RPMI formulation
700 without methionine, arginine and lysine (GIBCO), with 20% dialyzed FBS (GIBCO),
701 200 mg ml^{-1} L-proline) for 45 min. The cells were pelleted and cultured in
702 intermediate (depletion medium supplemented with 2H4-lysine, 13C6-arginine and
703 AHA) or heavy (depletion medium supplemented with 15N213C6-lysine, 15N413C6-
704 arginine and AHA) labelling medium for three hours. Cells were pelleted and lysed in
705 lysis buffer (8 M urea, 0.3 M HEPES, 0.75 M NaCl and 6.2% CHAPS detergent)
706 including protease inhibitor cocktail without EDTA (Roche) and sonicated on ice
707 using probe sonicator (Branson). Equal amounts of pre-cleared heavy and
708 intermediate SILAC labelled lysates were merged.

709 The nascent proteins were enriched with alkyne agarose resin slurry (Click-iT®
710 Protein Enrichment Kit, Thermo Fischer Scientific). On-beads digestion was
711 performed by overnight digestion with 5 µg of trypsin at 37°C in digestion buffer (100
712 mM ammonium bicarbonate in ULCMS water) in a shaking incubator. The samples
713 were centrifuged for 5 min (1,000 g, RT) and the supernatant with digested peptides
714 was collected. Peptides were desalted using an Oasis PRiME HKB mElution Plate
715 according to manufacturer's instructions. The samples were vacuum dried and
716 dissolved in 0.1% formic acid. High pH Reversed Phase fractionation was done on
717 Infinity 1260 LC system (Agilent) with Gemini® 3 µm C18 column (Phenomonex).
718 Separation occurred along 60 min linear gradient of buffer A (20 mM ammonium
719 formate pH 10) and buffer B (100% acetonitrile). Samples were dried and dissolved in
720 0.1% formic acid.

721 MS was performed on Q-Exactive HF or Orbitrap Fusion mass spectrophotometers
722 connected to EASY-nLC™ 1200 (Thermo Scientific). Peptides were separated with a
723 C18 UPLC column (Thermo Scientific). The Q Exactive HF mass spectrometer was
724 operated in data-dependent mode, acquiring one survey MS scan in the orbitrap
725 followed by up to 20 fragmentation scans (TOP20) of the most abundant ions
726 analyzed in the MS by HCD fragmentation. Orbitrap Fusion was operated using
727 Orbitrap as MS1 analyzer and Ion Trap as MS2 analyzer.

728 The raw mass spectrometry data were processed with MaxQuant. A minimum of 2
729 peptides was required for protein identification and the false discovery rate (FDR) at
730 peptide and protein level was set to 0.01. R/Bioconductor was used to calculate the
731 percentages of SILAC MS/MS spectra as a percentage of the total MS/MS per protein
732 group. SILAC ratios below the threshold of 0.1 were removed. The SILAC ratios
733 were inverted to account for SILAC label swap between replicate experiments.
734 Subsequently, ratios were log2 transformed and corrected by the median of the log2
735 ratios to obtain filtered and normalized ratios for further analysis. Proteins quantified
736 in both replicates were subjected to differential expression analysis by Limma R
737 package. Multiple test correction was applied according to Benjamini-Hochberg
738 procedure. Adjusted p values equal or lower than 0.05 pointed to statistically
739 significant protein expression change.

740 **SNORD127$^{+/-}$ generation.** SNORD127 heterozygous knockout (SNORD127$^{+/-}$) lines
741 were generated either by transducing inducible Cas9-expressing cells with lentiviral
742 constructs expressing paired sgRNA specific to SNORD127 locus (for Kasumi-1) or
743 by transfecting Cas9 protein and synthetic paired sgRNA (Synthego) (for OCI-
744 AML2). To generate doxycycline inducible Cas9-expressing cells, Kasumi-1 cells
745 were transduced with Lenti-iCas9-neo and selected with 1 mg ml^{-1} G418 for 2 weeks.
746 Cells were treated with 100 ng ml^{-1} doxycycline to induced Cas9-P2A-GFP
747 expression, and single cells with high Cas9-P2A-GFP expression were selected and
748 expanded as parent cells to make SNORD127 knockout. Kasumi-1 iCas9 cells were
749 infected with pDECKO lentivirus expressing paired sgRNA and FACS-sorted for
750 mCherry positive cells. To induce SNORD127 knockout in the selected population,
751 Cas9 expression was induced by treating cells with 100 ng ml^{-1} doxycycline for 4
752 days. Single clones were picked and expanded to screen SNORD127 deletion.

753 For SNORD127 knockout in OCI-AML2 cells, Cas9-Cy3 protein (Cat. CP06-100,
754 PNA Bio) and synthetic SNOR127 paired sgRNA (Synthego) were electroporated
755 into OCI-AML2 cells with Neon transfection system (Thermo Scientific). Briefly,
756 1µg of sgRNA was incubated with 1µg Cas9-Cy3 protein for 15 min at room
757 temperature in 2 µl PBS without Ca^{2+} and Mg^{2+}. The cells were washed with PBS
758 (without Ca^{2+} and Mg^{2+}) and resuspended in resuspension buffer R to a density of 2 x
759 10^7 cells ml^{-1}. A total of 13 µl cells suspension was added to the pre-mixed 2 µl of the
760 Cas9 protein/sgRNA RNP. A volume of 10 µl cell/RNP mixture was used for
761 electroporation on Neon system. Afterwards, cells were cultured in 500 µl medium
762 (RPMI 1640 with 10% FBS) without antibiotics. Forty-eight hours later, single cells
763 were sorted into 96-well plate from Cy3 positive populations. Genomic DNA was
764 extracted from the single clones and the knockout clones were screened by
765 genotyping PCR with forward primer CTG TCA AAC TAG CCC GGC ATC and
766 reverse primer GGC AAC GCC TAT GCT TTT GTT T. All the knockouts were
767 further confirmed by Sanger sequencing. Single clones without any mutations in
768 SNORD127 loci were used as wildtype control clones.

769 **GSEA.** GSEA (Gene set enrichment analysis) was conducted using the GSEA
770 desktop application with from the Broad Institute. LSC_17 gene set contains a list of
771 17 genes generated in(61). The LSC_Up gene set was composed of 43 highly
772 expressed genes (RPKM > 1) which showed at least twofold increase in LSC^{high} vs.
773 LSC^{low} AMLs(62). The HEMATOPOIETIC_CELL_LINEAGE and
774 BROWN_MYELOID_CELL_DEVELOPMENT_UP gene set was downloaded from
775 GSEA molecular signature database. For FBL mRNA expression associated
776 signatures (Supplementary Figure 1B to D), we used our mRNA-Seq data from AML
777 patient samples and calculated the Pearson correlation between FBL mRNA with each
778 of other transcripts. The transcripts were then ranked from high to low correlation
779 score (from positive to negative correlation, shown "corr" and "anticorr" in Figures).
780 The pre-ranked gene list was applied to Gene Set Enrichment Analysis (GSEA) with
781 the indicated gene sets. For rRNA 2'-O-Me associated signatures, the AML patients
782 were divided into two group (high and low) according to the total 2'-O-Me score on
783 the relevant clusters or site. We then compared mRNA-Seq data of these two groups
784 to calculate fold change for each gene with their mean value in each group. The genes
785 were ranked based on fold change and applied to GESA analysis with the indicated
786 gene set.

787 **Gene ontology analysis.** Gene ontology analysis was performed with ShinyGo
788 (http://bioinformatics.sdstate.edu/go/).

789 **Metabolite screening by GC/MS.** Semi-targeted metabolites screening was
790 performed with Gas Chromatography/Mass Spectrometry (GC/MS) analysis. Briefly,
791 frozen pellets were extracted in 180 µl of 100% MeOH for 15 min at 70 °C with
792 vigorous shaking. As internal standard 10 µl Ribitol (0.2 mg ml^{-1}) was added to each
793 sample. After the addition of 100 µl chloroform samples were shaken at 37 °C for 5
794 min. To separate polar and organic phases, 200 µl water were added and samples
795 were centrifuged for 10 min at 11,000 g. For derivatization, 300 µl of the polar (upper)
796 phase were transferred to a fresh tube and dried in a speed-vac (vacuum concentrator)
797 without heating. GC/MS-QP2010 Plus (Shimadzu®) fitted with a Zebron ZB 5MS
798 column (Phenomenex®) was used for GC/MS analysis. The GC was operated with an
799 injection temperature of 230 °C and 2 µl sample were injected with split mode. The
800 MS was operated with ion source and interface temperatures of 250 °C, a solvent cut
801 time of 6.3 min and a scan range (m/z) of 40-1000 with an event time of 0.3 sec. The
802 "GCMS solution" software (Shimadzu®) was used for data processing. Metabolite set
803 enrichment analysis was performed with MetaboAnalyst5.0.

804 **Targeted metabolites via UPLC.** Target analysis for amino acids, thiols and
805 metabolites in tricarboxylic acid cycle (TCA cycle) was conducted by ultra
806 performance liquid chromatography (UPLC). Free amino acids and thiols were
807 extracted from frozen cell pellets with 0.3 ml of 0.1 M HCl in an ultrasonic ice-bath
808 for 10 min. The resulting extracts were centrifuged twice for 10 min at 4 °C and
809 16,400 g to remove cell debris. Amino acids were derivatized with AccQ-Tag reagent
810 (Waters) and determined as described in Weger et al(63). Total glutathione was

811 quantified by reducing disulfides with DTT followed by thiol derivatization with the
812 fluorescent dye monobromobimane (thiolyte, calbiochem). For quantification of
813 GSSG, free thiols were first blocked by NEM followed by DTT reduction and
814 monobromobimane derivatization. GSH equivalents were calculated by subtracting
815 GSSG from total glutathione levels. Derivatization was performed as described in
816 Wirtz et al(64). UPLC-FLR analysis was carried out using an Acquity H-class UPLC
817 system. Separation was achieved with a binary gradient of buffer A (100 mM
818 potassium acetate pH 5.3) and solvent B (acetonitrile). The column (Acquity BEH
819 Shield RP18 column, Waters) was maintained at 45 °C and sample temperature was
820 kept constant at 14 °C. Monobromobimane conjugates were detected by fluorescence
821 at 480 nm after excitation at 380 nm and quantified using ultrapure standards (Sigma).
822 Determination of organic acids was adapted from Uran et al(65). In brief, cell pellets
823 were extracted in 0.2 ml ice-cold methanol with sonication on ice. A volume of 50 µl
824 extract was mixed with 25 µl 140 mM 3-Nitrophenylhydrazine hydrochloride (Sigma-
825 Aldrich), 25 µl methanol and 100 µl 50 mM Ethyl-3-(3-dimethylaminopropyl)
826 carbodiimide hydrochloride (Sigma-Aldrich) and incubated for 20 min at 60 °C.
827 Separation was carried out on the above described UPLC system coupled to a QDa
828 mass detector (Waters) using an Acquity HSS T3 column (Waters). Separation of
829 derivates was achieved by increasing the concentration of 0.1% formic acid in
830 acetonitrile (B) in 0.1% formic acid in water (A) at 0.55 ml min^{-1}. Mass signals for the
831 following compounds were detected in single ion record (SIR) mode using negative
832 detector polarity and 0.8 kV capillary voltage: Lactate (224.3 m/z; 25 V CV), malate
833 (403.3 m/z; 25 V CV), succinate (387.3 m/z; 25 CV), fumarate (385.3 m/z; 30 V),
834 citrate (443.3 m/z; 10 V), pyruvate (357.3 m/z; 15 V) and ketoglutarate (550.2 m/z; 25
835 CV). Data acquisition and processing was performed with the Empower3 software
836 suite (Waters).

837 **Ribosome purification by sucrose gradient.** Purification of 80S ribosomes of the
838 SNORD127$^{+/+}$ and SNORD127$^{+/-}$ cells were conducted by sucrose gradient
839 centrifugation. In brief, cells were resuspended in lysis buffer (20 mM HEPES pH
840 7.4, 100 mM KOAc, 7.5 mM $Mg(OAc)_2$, 1 mM DTT, 0.5% NP-40) with protease
841 inhibitor cocktail (Cat.11873580001, Roche). Cell lysates were incubated on ice for
842 10 min and pushed through a 26G needle. Cell debris was discarded by centrifugation
843 at 12,000 g for 15 min at 4 °C, and the cytoplasmic fraction without any lipids was
844 loaded onto 1M sucrose cushion (50 mM HEPES pH 7.4, 100 mM KOAc, 7.5 mM
845 $Mg(OAc)_2$, 5 mM β-mercaptoethanol, 1 M sucrose, 0.1% NP-40). The ribosome-
846 enriched pellet was obtained by centrifugation at 100,000 rpm at 4 °C for 45 min in
847 TLA110 rotor. The pellet was resuspended in ribosome storage buffer (20 mM
848 HEPES pH 7.4, 100 mM KOAc, 5 mM $Mg(OAc)_2$, 2 mM DTT). Ribosome particles
849 were purified on a 10 - 40% sucrose gradient using a SW40 rotor at 16,700 rpm for 18
850 h at 4 °C. Fractions containing 80S ribosomes were collected into chilled 2 ml tubes
851 on ice. The 80S ribosomes were concentrated at 2,000 rpm in 15 ml Pierce™ Protein
852 Concentrator, 100K MWCO (Cat. 88533, Thermo Scientific) to 500 µl, diluted with
853 Ribosome Storage Buffer to 5 ml and concentrated again to 500 µl. The

854 concentration-dilution was repeated 4 times to remove sucrose traces. The ribosomal
855 pellet was resuspended in ribosome storage buffer and stored at −80 °C until further
856 use.

857 **Cryo-EM structure analysis of ribosome.** Electron microscopy and image processing.
858 After ribosome purification by sucrose gradient, a final concentration 0.05% NP-40
859 was added to the samples. Purified 3.5 µl of sample was applied to pre-coated (2 nm)
860 R3/3 holey-carbon-supported copper grids (Quantifoil), blotted for 2-3 s at 4 °C and
861 plunge-frozen in liquid ethane using an FEI Vitrobot Mark IV (FEI Company). Data
862 were collected on a Titan Krios operated at 300 keV. All data were collected with a
863 pixel size of 1.059 Å/pixel and within a defocus range of -0.8 to -2.5 µm using a K2
864 Summit direct electron detector under low-dose conditions with a total dose of 44 e-
865 /Å2. Original image stacks were dose weighted, aligned, summed and drift-corrected
866 using MotionCor2(66). Contrast-transfer function (CTF) parameters and resolutions
867 were estimated for each micrograph using CTFFIND4 and GCTF, respectively[67,68].
868 Micrographs with an estimated resolution better than 5 Å and an astigmatism below
869 5% were manually screened for contamination or carbon rupture.

870 References free particle picking was carried out using Gautomatch. In total, 582,101
871 particles were picked from 12,443 good micrographs of the SNORD127$^{+/+}$ cell dataset
872 and 538,797 particles were picked from 7,533 good micrographs of the SNORD127$^{+/-}$
873 cell dataset. After 2D classification, a total number 188,471 particles and 394,983
874 particles of the SNORD127$^{+/+}$ and SNORD127$^{+/-}$ cell dataset, respectively, were
875 selected for the following 3D classification and 3D Refinement in Relion 3.1(69). The
876 final class which contained the most particle number and display higher resolution
877 was picked since we aimed for high resolution map to see the 2'-O methylation. To
878 improve the overall resolution and local resolution, CTF refinement and multibody
879 refinement were applied for the picked classes. In general, the 80S ribosome was
880 divided into three bodies: the 60S ribosome, the 40S ribosome body and the 40S
881 ribosome head. To better illustrate the map, local resolution filter was carried out for
882 all the three bodies.

883 Model building and refinement. The human 80S ribosome structure (PDB ID: 6ZMI)
884 was used as initial references to do rigid body fit, followed by manual adjustment in
885 Coot (such as remove NSP1 protein)(70,71). In the case of the model from
886 SNORD127$^{+/-}$ cell, E site tRNA and LYAR were removed. Since most of the region
887 has sufficient resolution to distinguish 2-O methylation, all the modified bases were
888 manually built. In the center of the structure, magnesium and water molecules were
889 visible, thus we also manually built them. The final models were real-space refined
890 with secondary structure restraints using the PHENIX suite(72). Final model
891 evaluation was performed with MolProbity(73). Maps and models were visualized
892 and figures created with ChimeraX(74).

893

Statistics. No statistical method was used to predetermine sample size. The experiments were not randomized. Animals with the same gender and age were used in paired groups. The investigators were not blinded to allocation during experiments and outcome assessment**.** To test statistical significance between samples from two different groups two-tailed Student's t tests were used. When comparing samples from the same patient paired t tests were applied. Data are represented as means ± s.d. unless otherwise indicated. Sample sizes and significance are shown in corresponding figure legends. Relative importance of individual covariates in multivariate logistic regression models was estimated by examining Pearson's chi-squared test. The survival curves were constructed according to the Kaplan-Meier with the log-rank test. Bioinformatics statistical analysis was performed using R.

Data availability. The sequencing data has been deposited in the GEO SuperSeries under accession number GSE184721, GSE184722, GSE184724, GSE184727 and GSE185489. Ribosome Cryo-EM structures from SNORD127$^{+/+}$ and SNORD127$^{+/-}$ leukemia cells have been deposited in electron microscopy data bank (EMD) and Protein Data Bank (PDB) under accession number EMD_33329, PDB7XNX and EMD_33330, PDB7XNY. Ribosome structure to visualize the distribution of 2'-O-Me sites is from PDB 4UG0. Previously published human FBL structure is from PDB 5GIO. The mass spectrometry proteomics data have been deposited to the ProteomeXchange Consortium via the PRIDE partner repository with the dataset identifier PXD029527.

Code availability. All codes and scripts used in paper are available upon reasonable request.

Author contributions:

F.Z. designed the study, performed experiments and analzed the data; N.A. designed and performed *in vivo* engrafting experiments and analyzed the data; Y.L. generated SNORD127 knockout cell lines, performed CFU assay and structure analysis; C.R. performed bioinformatic analyses with conceptual input from F.Z. and C.M-T; J.C. and R.B. determined ribosome structure; D.F. and J.K. generated and analyzed the nascent proteome data; A-K.W. and I.J. helped to design and perform AML PDX transplantation experiments; Y.H. helped with data analysis and discussion; Y.X. helped with flow cytometry analysis; T.S. helped with animal experiments. M.L. performed experiments. S.G., C.P., T.O., H.S., C.B. and M.F. discussed the results and advised on research; C.R., M.B. and C.T. provided AML samples and clinical data; S.R. provided AML samples and proteome data; C.M-T. designed with F.Z. the overall study and supervised it. A.T. helped to design and supervise parts of the study; F.Z. wrote the manuscript with A.T. and C.M-T.

Acknowledgements. We thank Stefanie Hofmann and Dr. Volker Eckstein for flow cytometry cell sorting. We thank the Metabolomics Core Technology Platform of the Excellence Cluster CellNetworks for support with metabolite quantification. We

thank K. Reifenberg, P. Prückl, M. Durst, A. Rathgeb, and animal caretaker of the DKFZ Central Animal Laboratory for excellent animal welfare and husbandry, members of the DKFZ Core Facility Flow Cytometry for technical assistance, Dr. Darja Karpova and Prof. Halvard B. Bönig (IHBT, Frankfurt am Main) for providing the AML patient samples. This work was supported by Deutsche Forschungsgemeinschaft (DFG) ZH 831/1-1 (F. Zhou), DFG MU 1328/15-1, MU 1328/9-2, MU 1328/18-1 (C. Müller-Tidow), DFG RA 3166/2-1 (S. Raffel), DFG SPP2036, FOR2674 and SFB873 (A. Trumpp). Deutsche Krebshilfe 70113908, 111286, 70112974 (C. Müller-Tidow), Deutsche José-Carreras-Leukämie-Stiftung DJCLS 22R/2017, DJCLS R 13/04 (C. Müller-Tidow) and Sander Stiftung Nr. 2017.004.1 (C. Müller-Tidow), BMBF 01ZX1911D (S. Raffel). ERC advanced Grant SHATTER-AML 101055270 (A. Trumpp), DKTK joint funding project "RiskY-AML" (A. Trumpp) and the Dietmar Hopp Foundation (A. Trumpp). For the publication fee we acknowledge financial support by DFG within the funding programme "Open Access Publikationskosten" as well as by Heidelberg University.

Competing interest: No competing interest to be declared.

References:

1. Bonnet D, Dick JE. Human acute myeloid leukemia is organized as a hierarchy that originates from a primitive hematopoietic cell. Nature medicine **1997**;3(7):730-7 doi 10.1038/nm0797-730.
2. Chua BA, Van Der Werf I, Jamieson C, Signer RAJ. Post-Transcriptional Regulation of Homeostatic, Stressed, and Malignant Stem Cells. Cell stem cell **2020**;26(2):138-59 doi 10.1016/j.stem.2020.01.005.
3. Saba JA, Liakath-Ali K, Green R, Watt FM. Translational control of stem cell function. Nature reviews Molecular cell biology **2021**;22(10):671-90 doi 10.1038/s41580-021-00386-2.
4. Schwanhausser B, Busse D, Li N, Dittmar G, Schuchhardt J, Wolf J*, et al.* Global quantification of mammalian gene expression control. Nature **2011**;473(7347):337-42 doi 10.1038/nature10098.
5. Khan Z, Ford MJ, Cusanovich DA, Mitrano A, Pritchard JK, Gilad Y. Primate transcript and protein expression levels evolve under compensatory selection pressures. Science **2013**;342(6162):1100-4 doi 10.1126/science.1242379.
6. Signer RA, Magee JA, Salic A, Morrison SJ. Haematopoietic stem cells require a highly regulated protein synthesis rate. Nature **2014**;509(7498):49-54 doi 10.1038/nature13035.
7. Blanco S, Bandiera R, Popis M, Hussain S, Lombard P, Aleksic J*, et al.* Stem cell function and stress response are controlled by protein synthesis. Nature **2016**;534(7607):335-40 doi 10.1038/nature18282.
8. Sanchez CG, Teixeira FK, Czech B, Preall JB, Zamparini AL, Seifert JR*, et al.* Regulation of Ribosome Biogenesis and Protein Synthesis Controls Germline Stem Cell Differentiation. Cell stem cell **2016**;18(2):276-90 doi 10.1016/j.stem.2015.11.004.
9. Zismanov V, Chichkov V, Colangelo V, Jamet S, Wang S, Syme A*, et al.* Phosphorylation of eIF2alpha Is a Translational Control Mechanism Regulating

Muscle Stem Cell Quiescence and Self-Renewal. Cell stem cell **2016**;18(1):79-90 doi 10.1016/j.stem.2015.09.020.

10. Harding HP, Novoa I, Zhang Y, Zeng H, Wek R, Schapira M*, et al.* Regulated translation initiation controls stress-induced gene expression in mammalian cells. Molecular cell **2000**;6(5):1099-108 doi 10.1016/s1097-2765(00)00108-8.

11. Teslaa T, Teitell MA. Pluripotent stem cell energy metabolism: an update. The EMBO journal **2015**;34(2):138-53 doi 10.15252/embj.201490446.

12. Khajuria RK, Munschauer M, Ulirsch JC, Fiorini C, Ludwig LS, McFarland SK*, et al.* Ribosome Levels Selectively Regulate Translation and Lineage Commitment in Human Hematopoiesis. Cell **2018**;173(1):90-103 e19 doi 10.1016/j.cell.2018.02.036.

13. Ruggero D, Grisendi S, Piazza F, Rego E, Mari F, Rao PH*, et al.* Dyskeratosis congenita and cancer in mice deficient in ribosomal RNA modification. Science **2003**;299(5604):259-62 doi 10.1126/science.1079447.

14. Decatur WA, Fournier MJ. rRNA modifications and ribosome function. Trends in biochemical sciences **2002**;27(7):344-51 doi 10.1016/s0968-0004(02)02109-6.

15. Polikanov YS, Melnikov SV, Soll D, Steitz TA. Structural insights into the role of rRNA modifications in protein synthesis and ribosome assembly. Nature structural & molecular biology **2015**;22(4):342-4 doi 10.1038/nsmb.2992.

16. Natchiar SK, Myasnikov AG, Kratzat H, Hazemann I, Klaholz BP. Visualization of chemical modifications in the human 80S ribosome structure. Nature **2017**;551(7681):472-7 doi 10.1038/nature24482.

17. Burakovsky DE, Prokhorova IV, Sergiev PV, Milon P, Sergeeva OV, Bogdanov AA*, et al.* Impact of methylations of m2G966/m5C967 in 16S rRNA on bacterial fitness and translation initiation. Nucleic acids research **2012**;40(16):7885-95 doi 10.1093/nar/gks508.

18. Sloan KE, Warda AS, Sharma S, Entian KD, Lafontaine DLJ, Bohnsack MT. Tuning the ribosome: The influence of rRNA modification on eukaryotic ribosome biogenesis and function. RNA biology **2017**;14(9):1138-52 doi 10.1080/15476286.2016.1259781.

19. Sharma S, Lafontaine DLJ. 'View From A Bridge': A New Perspective on Eukaryotic rRNA Base Modification. Trends in biochemical sciences **2015**;40(10):560-75 doi 10.1016/j.tibs.2015.07.008.

20. Kiss-Laszlo Z, Henry Y, Bachellerie JP, Caizergues-Ferrer M, Kiss T. Site-specific ribose methylation of preribosomal RNA: a novel function for small nucleolar RNAs. Cell **1996**;85(7):1077-88 doi 10.1016/s0092-8674(00)81308-2.

21. Cavaille J, Nicoloso M, Bachellerie JP. Targeted ribose methylation of RNA in vivo directed by tailored antisense RNA guides. Nature **1996**;383(6602):732-5 doi 10.1038/383732a0.

22. Zhou F, Liu Y, Rohde C, Pauli C, Gerloff D, Kohn M*, et al.* AML1-ETO requires enhanced C/D box snoRNA/RNP formation to induce self-renewal and leukaemia. Nature cell biology **2017**;19(7):844-55 doi 10.1038/ncb3563.

23. Pauli C, Liu Y, Rohde C, Cui C, Fijalkowska D, Gerloff D*, et al.* Site-specific methylation of 18S ribosomal RNA by SNORD42A is required for acute myeloid leukemia cell proliferation. Blood **2020**;135(23):2059-70 doi 10.1182/blood.2019004121.

24. Jansson MD, Hafner SJ, Altinel K, Tehler D, Krogh N, Jakobsen E*, et al.* Regulation of translation by site-specific ribosomal RNA methylation. Nature structural & molecular biology **2021**;28(11):889-99 doi 10.1038/s41594-021-00669-4.

25. Krogh N, Jansson MD, Hafner SJ, Tehler D, Birkedal U, Christensen-Dalsgaard M*, et al.* Profiling of 2'-O-Me in human rRNA reveals a subset of fractionally modified positions and provides evidence for ribosome heterogeneity. Nucleic acids research **2016**;44(16):7884-95 doi 10.1093/nar/gkw482.

26. Erales J, Marchand V, Panthu B, Gillot S, Belin S, Ghayad SE*, et al.* Evidence for rRNA 2'-O-methylation plasticity: Control of intrinsic translational capabilities of human ribosomes. Proceedings of the National Academy of Sciences of the United States of America **2017**;114(49):12934-9 doi 10.1073/pnas.1707674114.
27. Krogh N, Asmar F, Come C, Munch-Petersen HF, Gronbaek K, Nielsen H. Profiling of ribose methylations in ribosomal RNA from diffuse large B-cell lymphoma patients for evaluation of ribosomes as drug targets. NAR cancer **2020**;2(4):zcaa035 doi 10.1093/narcan/zcaa035.
28. Marcel V, Kielbassa J, Marchand V, Natchiar KS, Paraqindes H, Nguyen Van Long F*, et al.* Ribosomal RNA 2'O-methylation as a novel layer of inter-tumour heterogeneity in breast cancer. NAR cancer **2020**;2(4):zcaa036 doi 10.1093/narcan/zcaa036.
29. Dick JE. Stem cell concepts renew cancer research. Blood **2008**;112(13):4793-807 doi 10.1182/blood-2008-08-077941.
30. Raffel S, Falcone M, Kneisel N, Hansson J, Wang W, Lutz C*, et al.* BCAT1 restricts alphaKG levels in AML stem cells leading to IDHmut-like DNA hypermethylation. Nature **2017**;551(7680):384-8 doi 10.1038/nature24294.
31. Marchand V, Blanloeil-Oillo F, Helm M, Motorin Y. Illumina-based RiboMethSeq approach for mapping of 2'-O-Me residues in RNA. Nucleic acids research **2016**;44(16):e135 doi 10.1093/nar/gkw547.
32. Raffel S, Klimmeck D, Falcone M, Demir A, Pouya A, Zeisberger P*, et al.* Quantitative proteomics reveals specific metabolic features of acute myeloid leukemia stem cells. Blood **2020**;136(13):1507-19 doi 10.1182/blood.2019003654.
33. Khatter H, Myasnikov AG, Natchiar SK, Klaholz BP. Structure of the human 80S ribosome. Nature **2015**;520(7549):640-5 doi 10.1038/nature14427.
34. Yang Z, Lin J, Ye K. Box C/D guide RNAs recognize a maximum of 10 nt of substrates. Proceedings of the National Academy of Sciences of the United States of America **2016**;113(39):10878-83 doi 10.1073/pnas.1604872113.
35. Eichelbaum K, Winter M, Berriel Diaz M, Herzig S, Krijgsveld J. Selective enrichment of newly synthesized proteins for quantitative secretome analysis. Nature biotechnology **2012**;30(10):984-90 doi 10.1038/nbt.2356.
36. Jones CL, Stevens BM, D'Alessandro A, Reisz JA, Culp-Hill R, Nemkov T*, et al.* Inhibition of Amino Acid Metabolism Selectively Targets Human Leukemia Stem Cells. Cancer cell **2018**;34(5):724-40 e4 doi 10.1016/j.ccell.2018.10.005.
37. Jones CL, Stevens BM, D'Alessandro A, Culp-Hill R, Reisz JA, Pei S*, et al.* Cysteine depletion targets leukemia stem cells through inhibition of electron transport complex II. Blood **2019**;134(4):389-94 doi 10.1182/blood.2019898114.
38. Presnyak V, Alhusaini N, Chen YH, Martin S, Morris N, Kline N*, et al.* Codon optimality is a major determinant of mRNA stability. Cell **2015**;160(6):1111-24 doi 10.1016/j.cell.2015.02.029.
39. Hanson G, Coller J. Codon optimality, bias and usage in translation and mRNA decay. Nature reviews Molecular cell biology **2018**;19(1):20-30 doi 10.1038/nrm.2017.91.
40. Wu Q, Medina SG, Kushawah G, DeVore ML, Castellano LA, Hand JM*, et al.* Translation affects mRNA stability in a codon-dependent manner in human cells. eLife **2019**;8 doi 10.7554/eLife.45396.
41. Najafabadi HS, Goodarzi H, Salavati R. Universal function-specificity of codon usage. Nucleic acids research **2009**;37(21):7014-23 doi 10.1093/nar/gkp792.
42. Akashi H. Translational selection and yeast proteome evolution. Genetics **2003**;164(4):1291-303.
43. Frumkin I, Lajoie MJ, Gregg CJ, Hornung G, Church GM, Pilpel Y. Codon usage of highly expressed genes affects proteome-wide translation efficiency. Proceedings of

the National Academy of Sciences of the United States of America **2018**;115(21):E4940-E9 doi 10.1073/pnas.1719375115.

44. Yang JH, Zhang XC, Huang ZP, Zhou H, Huang MB, Zhang S*, et al.* snoSeeker: an advanced computational package for screening of guide and orphan snoRNA genes in the human genome. Nucleic acids research **2006**;34(18):5112-23 doi 10.1093/nar/gkl672.

45. Maden BE, Salim M. The methylated nucleotide sequences in HELA cell ribosomal RNA and its precursors. Journal of molecular biology **1974**;88(1):133-52 doi 10.1016/0022-2836(74)90299-x.

46. Miyazawa N, Yoshikawa H, Magae S, Ishikawa H, Izumikawa K, Terukina G*, et al.* Human cell growth regulator Ly-1 antibody reactive homologue accelerates processing of preribosomal RNA. Genes to cells : devoted to molecular & cellular mechanisms **2014**;19(4):273-86 doi 10.1111/gtc.12129.

47. Li H, Wang B, Yang A, Lu R, Wang W, Zhou Y*, et al.* Ly-1 antibody reactive clone is an important nucleolar protein for control of self-renewal and differentiation in embryonic stem cells. Stem cells **2009**;27(6):1244-54 doi 10.1002/stem.55.

48. Watanabe-Susaki K, Takada H, Enomoto K, Miwata K, Ishimine H, Intoh A*, et al.* Biosynthesis of ribosomal RNA in nucleoli regulates pluripotency and differentiation ability of pluripotent stem cells. Stem cells **2014**;32(12):3099-111 doi 10.1002/stem.1825.

49. Thoreen CC, Chantranupong L, Keys HR, Wang T, Gray NS, Sabatini DM. A unifying model for mTORC1-mediated regulation of mRNA translation. Nature **2012**;485(7396):109-13 doi 10.1038/nature11083.

50. Hsieh AC, Liu Y, Edlind MP, Ingolia NT, Janes MR, Sher A*, et al.* The translational landscape of mTOR signalling steers cancer initiation and metastasis. Nature **2012**;485(7396):55-61 doi 10.1038/nature10912.

51. Tahmasebi S, Jafarnejad SM, Tam IS, Gonatopoulos-Pournatzis T, Matta-Camacho E, Tsukumo Y*, et al.* Control of embryonic stem cell self-renewal and differentiation via coordinated alternative splicing and translation of YY2. Proceedings of the National Academy of Sciences of the United States of America **2016**;113(44):12360-7 doi 10.1073/pnas.1615540113.

52. Roundtree IA, Evans ME, Pan T, He C. Dynamic RNA Modifications in Gene Expression Regulation. Cell **2017**;169(7):1187-200 doi 10.1016/j.cell.2017.05.045.

53. Blair JD, Hockemeyer D, Doudna JA, Bateup HS, Floor SN. Widespread Translational Remodeling during Human Neuronal Differentiation. Cell reports **2017**;21(7):2005-16 doi 10.1016/j.celrep.2017.10.095.

54. Ingolia NT, Lareau LF, Weissman JS. Ribosome profiling of mouse embryonic stem cells reveals the complexity and dynamics of mammalian proteomes. Cell **2011**;147(4):789-802 doi 10.1016/j.cell.2011.10.002.

55. Vick B, Rothenberg M, Sandhofer N, Carlet M, Finkenzeller C, Krupka C*, et al.* An advanced preclinical mouse model for acute myeloid leukemia using patients' cells of various genetic subgroups and in vivo bioluminescence imaging. PloS one **2015**;10(3):e0120925 doi 10.1371/journal.pone.0120925.

56. Ebinger S, Zeller C, Carlet M, Senft D, Bagnoli JW, Liu WH*, et al.* Plasticity in growth behavior of patients' acute myeloid leukemia stem cells growing in mice. Haematologica **2020**;105(12):2855-60 doi 10.3324/haematol.2019.226282.

57. Terziyska N, Castro Alves C, Groiss V, Schneider K, Farkasova K, Ogris M*, et al.* In vivo imaging enables high resolution preclinical trials on patients' leukemia cells growing in mice. PloS one **2012**;7(12):e52798 doi 10.1371/journal.pone.0052798.

58. Lauria F, Tebaldi T, Bernabo P, Groen EJN, Gillingwater TH, Viero G. riboWaltz: Optimization of ribosome P-site positioning in ribosome profiling data. PLoS computational biology **2018**;14(8):e1006169 doi 10.1371/journal.pcbi.1006169.
59. Loayza-Puch F, Rooijers K, Buil LC, Zijlstra J, Oude Vrielink JF, Lopes R*, et al.* Tumour-specific proline vulnerability uncovered by differential ribosome codon reading. Nature **2016**;530(7591):490-4 doi 10.1038/nature16982.
60. Liu Q, Shvarts T, Sliz P, Gregory RI. RiboToolkit: an integrated platform for analysis and annotation of ribosome profiling data to decode mRNA translation at codon resolution. Nucleic acids research **2020**;48(W1):W218-W29 doi 10.1093/nar/gkaa395.
61. Ng SW, Mitchell A, Kennedy JA, Chen WC, McLeod J, Ibrahimova N*, et al.* A 17-gene stemness score for rapid determination of risk in acute leukaemia. Nature **2016**;540(7633):433-7 doi 10.1038/nature20598.
62. Pabst C, Bergeron A, Lavallee VP, Yeh J, Gendron P, Norddahl GL*, et al.* GPR56 identifies primary human acute myeloid leukemia cells with high repopulating potential in vivo. Blood **2016**;127(16):2018-27 doi 10.1182/blood-2015-11-683649.
63. Weger BD, Weger M, Gorling B, Schink A, Gobet C, Keime C*, et al.* Extensive Regulation of Diurnal Transcription and Metabolism by Glucocorticoids. PLoS genetics **2016**;12(12):e1006512 doi 10.1371/journal.pgen.1006512.
64. Wirtz M, Droux M, Hell R. O-acetylserine (thiol) lyase: an enigmatic enzyme of plant cysteine biosynthesis revisited in Arabidopsis thaliana. Journal of experimental botany **2004**;55(404):1785-98 doi 10.1093/jxb/erh201.
65. Uran S, Landmark KE, Hjellum G, Skotland T. Quantification of 13C pyruvate and 13C lactate in dog blood by reversed-phase liquid chromatography-electrospray ionization mass spectrometry after derivatization with 3-nitrophenylhydrazine. Journal of pharmaceutical and biomedical analysis **2007**;44(4):947-54 doi 10.1016/j.jpba.2007.04.001.
66. Zheng SQ, Palovcak E, Armache JP, Verba KA, Cheng Y, Agard DA. MotionCor2: anisotropic correction of beam-induced motion for improved cryo-electron microscopy. Nat Methods **2017**;14(4):331-2 doi 10.1038/nmeth.4193.
67. Rohou A, Grigorieff N. CTFFIND4: Fast and accurate defocus estimation from electron micrographs. Journal of structural biology **2015**;192(2):216-21 doi 10.1016/j.jsb.2015.08.008.
68. Zhang K. Gctf: Real-time CTF determination and correction. Journal of structural biology **2016**;193(1):1-12 doi 10.1016/j.jsb.2015.11.003.
69. Zivanov J, Nakane T, Forsberg BO, Kimanius D, Hagen WJ, Lindahl E*, et al.* New tools for automated high-resolution cryo-EM structure determination in RELION-3. eLife **2018**;7 doi 10.7554/eLife.42166.
70. Thoms M, Buschauer R, Ameismeier M, Koepke L, Denk T, Hirschenberger M*, et al.* Structural basis for translational shutdown and immune evasion by the Nsp1 protein of SARS-CoV-2. Science **2020**;369(6508):1249-55 doi 10.1126/science.abc8665.
71. Emsley P, Cowtan K. Coot: model-building tools for molecular graphics. Acta crystallographica Section D, Biological crystallography **2004**;60(Pt 12 Pt 1):2126-32 doi 10.1107/S0907444904019158.
72. Adams PD, Afonine PV, Bunkoczi G, Chen VB, Davis IW, Echols N*, et al.* PHENIX: a comprehensive Python-based system for macromolecular structure solution. Acta crystallographica Section D, Biological crystallography **2010**;66(Pt 2):213-21 doi 10.1107/S0907444909052925.
73. Chen VB, Arendall WB, 3rd, Headd JJ, Keedy DA, Immormino RM, Kapral GJ*, et al.* MolProbity: all-atom structure validation for macromolecular crystallography. Acta

crystallographica Section D, Biological crystallography **2010**;66(Pt 1):12-21 doi 10.1107/S0907444909042073.

74. Goddard TD, Huang CC, Meng EC, Pettersen EF, Couch GS, Morris JH*, et al.* UCSF ChimeraX: Meeting modern challenges in visualization and analysis. Protein Sci **2018**;27(1):14-25 doi 10.1002/pro.3235.

1224 **Figure legends**

1225 Figure 1, The dynamic rRNA 2'-O-methylation associates with AML stemness.

1226 A, t-SNE analysis indicating cell type specific rRNA 2'-O-Methylation in normal
1227 human hematopoietic cells. HSPC, hematopoietic stem and progenitor cells.

1228 B, t-SNE analysis indicating distinct and heterogeneous rRNA 2'-O-methylation of
1229 human primary AMLs (n = 94).

1230 C, Variability of 2'-O-Me on each rRNA modification sites across human AMLs. The
1231 111 modification sites were ranked according to their 2'-O-Me diversity in AMLs.
1232 Red line shows average 2'-O-Me level of each site in AMLs, and grey indicates the
1233 range of 2'-O-Me.

1234 D, Unsupervised hierarchical clustering of pairwise correlation between rRNA
1235 dynamic sites based on 2'-O-Me in 94 AML patients. Each column lists the
1236 correlation of one site (in row) with all dynamic sites. Four dynamic clusters (DyMeC,
1237 black boxes) with co-occurrence in 2'-O-methylation were identified. rRNA sites in
1238 DyMeC 2 are labelled.

1239 E, Number of AML cases with maturation classification in groups with low and high
1240 2'-O-Me on DyMeC cluster 2. Immature, FAB M0 and M1 subtype; Mature, FAB M2
1241 to M6. P = 5.52E-04, Chi-Square test. Patients with no FAB subtype information were
1242 not included in each group.

1243 F, GSEA plot showing enrichment of LSC gene signatures in AML patients with
1244 higher total 2'-O-Me on DyMeC 2.

1245 G, Heatmap of 2'-O-Me clusters with increased modification in LSC, supervised by
1246 cell types. Samples are in columns; 2'-O-Me sites are in rows. Blue indicates DyMeC
1247 2 sites.

1248 H and I, Distribution of static (H) sites and the dynamic DyMeC 2 (I) on cryo-EM
1249 structure of human ribosome. Labelled in (H) are sites locating in ribosome conserved
1250 function centers, in (I) are LSC sites. E-site tRNA shown in red, rRNA and r-proteins
1251 in grey. PDB code for the structure is 4UGO. Modification sites from 4UGO are
1252 reannotated to rRNA sequence used for RiboMethSeq. DC, decoding center; PTC,
1253 peptidyl transferase center.

1254

1255

1256

1257

1258

Figure 2, The ribomethylome regulates AML stemness.

A, Changes in 2'-O-Me on each dynamic cluster after FBL knockdown in Kasumi-1 AML cells. n = 4 independent experiments. Indicated P value by unpaired Student's t-test.

B, Colony number formed by control (shCtrl) and FBL knockdown (shFBL) LSC populations. For FBL knockdown, a pool of two different FBL specific shRNAs was used. Indicated P value by unpaired Student's t-test.

C, Catalytic center of human FBL protein. Amino acid residues highlighted in purple are substrate binding sites. The substrate S-Adenosyl-L-homocysteine (SAH) is highlighted in green. Structure is from PDB 5GIO.

D, Western blot showing expression of V5-tagged exogenous wildtype and mutant FBL in FBL knockdown Kasumi-1 cells. Numbers on top indicate relative expression level of total FBL compared to that in control cells. ##V5-tagged exogenous FBL; #endogenous FBL.

E, Unsupervised clustering analysis of rRNA 2'-O-Me in FBL knockdown and rescued cells. The wildtype, but not mutant FBL restored rRNA 2'-O-methylation.

F, Colony formation assay showing rescue effect of wildtype and mutant FBL. Mean ± SD from n = 9 cultures from three experiments per group are given, statistical significance was assessed by Student's unpaired t-test.

G, Representative bioluminescence imaging of NSG mice transplanted with AML PDX cells overexpressing empty control, mutant (FBL^{Qua}) and wildtype FBL. Images were taken at the indicated time points after transplantation.

H, Summary of *in vivo* proliferation of PDX cells determined by bioluminescence imaging. Note that the signal from FBL^{WT} mice was approaching saturation at day 81. n = 4 for empty control, n = 5 for FBL^{Qua}, n = 3 for FBL^{WT}, *** P = 0.001; * P = 0.023; *n.s*, no significance, Student's unpaired t-test.

I, Absolute LSC frequency in bone marrow of each PDX estimated by *in vivo* limiting dilution assay. P = 0.0189, FBL^{WT} vs. Empty; P = 0.0006, FBL^{WT} vs. FBL^{Qua}, Chi-Square test.

1296 Figure 3, The ribomethylome regulates translation of amino acid transporters.

1297 A, Differentially translated proteins after FBL knockdown in Kasumi-1 AML cells.
1298 The difference in newly synthesized proteins (by nascent proteomics) was plotted
1299 against changes in mRNA (by mRNA-Seq). The red dots highlight differentially
1300 translated proteins, defined by $\log_2FC > 0.8$ (adjust $P < 0.05$) on nascent protein
1301 without changes on mRNA level.

1302 B, Gene ontology analysis of proteins less translated after FBL knockdown.

1303 C, Changes of amino acid transporters on nascent protein and mRNA level. Nascent
1304 proteins are shown in red, mRNA expression in grey.

1305 D, Western Blot showing protein levels of amino acid transporters in PDX cells
1306 transduced with empty vector or wildtype FBL. PDX cells were isolated from mice (n
1307 = 4 from empty control group and n = 3 from FBL^{WT} group) described in **Fig. 2H**.

1308 E, Abundance of cellular amino acid in PDX cells isolated from n = 3 mice each
1309 group.

1310 F, Comparison of ribosome P-site occupancy on each codon between control and FBL
1311 knockdown Kasumi-1 cells. Codons for the same amino acid are shown in same color.
1312 Dashed line indicates $\log_2FC = 0.3$.

1313 G, Distribution of codons with increased P-site ribosome occupancy in whole
1314 transcriptome, 1,000 random selected transcripts, all amino acid transporter genes and
1315 in amino acid transporter genes with decreased translation after FBL knockdown. The
1316 y axis indicates the proportion of genes within a given range of codons.

1317
1318
1319
1320
1321
1322
1323
1324
1325
1326
1327
1328
1329
1330
1331
1332
1333

Figure 4, Gm1447 determines leukemia stem cell activity.

A, Methylation levels on G1447 in 5 matched LSC and non-LSC fractions as described in **Fig. 1G**. Indicated P values by Student's paired t-test.

B, Variability of Gm1447 in primary AML samples. Shown are three patients with high, medium and low Gm1447, respectively. G1447 is shown in red, and U1442 with constitutive full methylation in human AMLs is shown in yellow. The arrow indicates +1 position to G1447 that the calculation of Gm1447 level (ScoreC) is based on (see method).

C, GSEA analysis showing that samples with high Gm1447 are enriched for LSC genes. Samples were split into two equal groups at median of Gm1447.

D, Comparison of rRNA 2'-O-Me in SNORD127$^{+/+}$ and SNORD127$^{+/-}$ Kasumi-1 cells.

E, Cryo-EM maps of 80S ribosome from SNORD127$^{+/+}$ and SNORD127$^{+/-}$ Kasumi-1 cells. Highlighted are 2'-O-Me density at G1447 and the decoding center of 40S ribosomal subunit. The arrow indicates density bump of 2'-O-Me on G1447 in SNORD127$^{+/+}$ cells.

F, Nascent proteomics from SNORD127$^{+/+}$ and SNORD127$^{+/-}$ Kasumi-1cells. Decreased nascent proteins in SNORD127$^{+/-}$ cells are labelled in blue, increased nascent proteins are in red.

G, Engraftment of SNORD127$^{+/+}$ and SNORD127$^{+/-}$ OCI-AML2 cells in NSG mice (percentages of leukemic cells among bone marrow cells; each dot represents one mouse; n = 12 mice for SNORD127$^{+/+}$ group, and n = 10 mice for SNORD127$^{+/-}$). Two different single clones per group were used for transplantation. Short horizonal line indicates mean, indicated P values by Student's unpaired t-test.

H, Survival of mice transplanted with SNORD127$^{+/+}$ and SNORD127$^{+/-}$ OCI-AML2 cells. n = 12 mice for control group, and n = 10 mice for SNORD127$^{+/-}$. Indicated P value by log-rank test.

I to K, Engraftment of primary AML cells AML03 (I), AML661 (J) and AML494 (K) transduced with empty vector or SNORD127. Each dot represents the bone marrow engraftment in one mouse. Short horizonal line indicates mean, indicated P values by Student's unpaired t-test.

L, Absolute LSC frequency in primary AML494 cells overexpressing empty vector or SNORD127 estimated by *in vivo* limiting dilution assay. P = 0.0015, Chi-Square test.

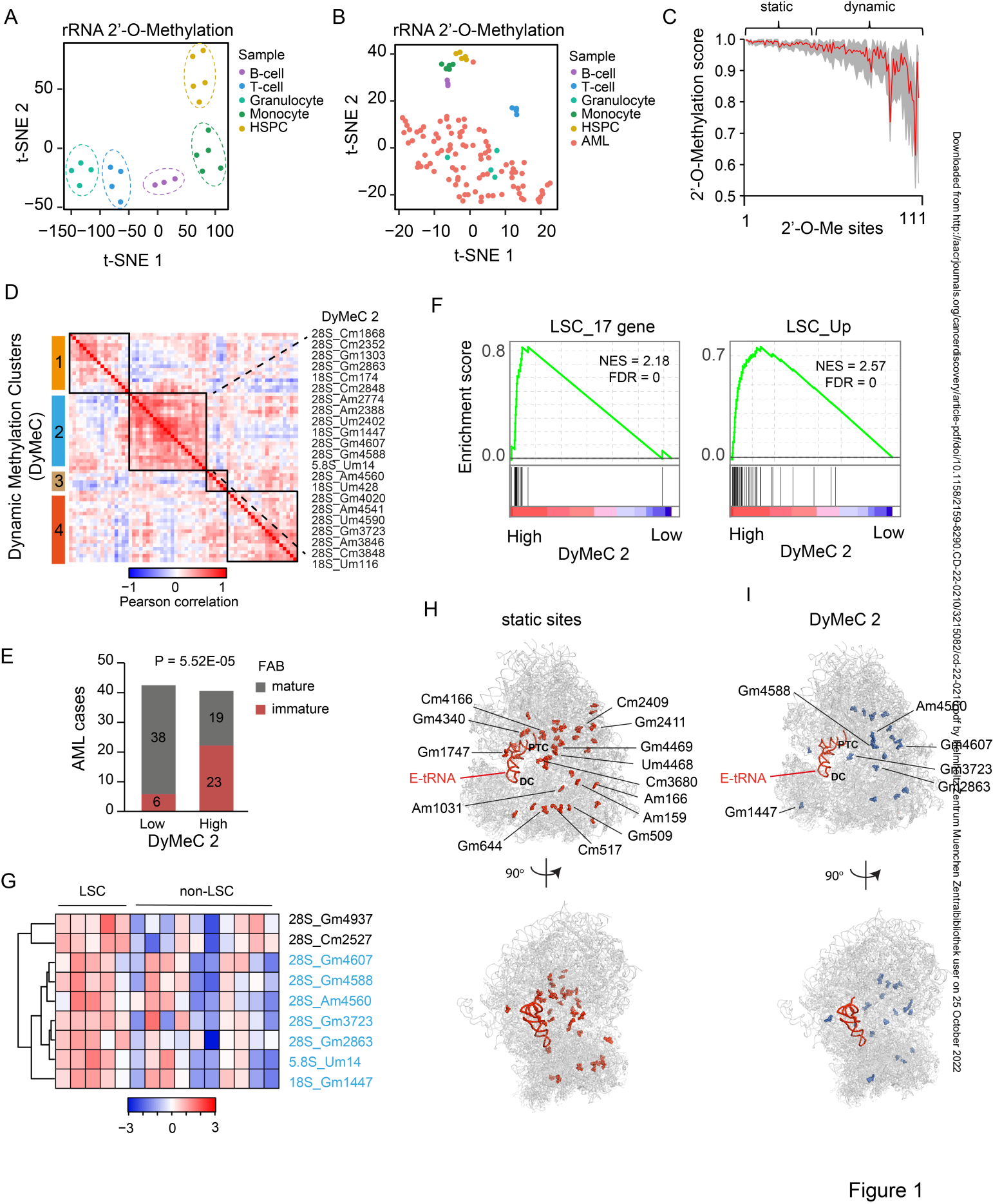

Figure 1

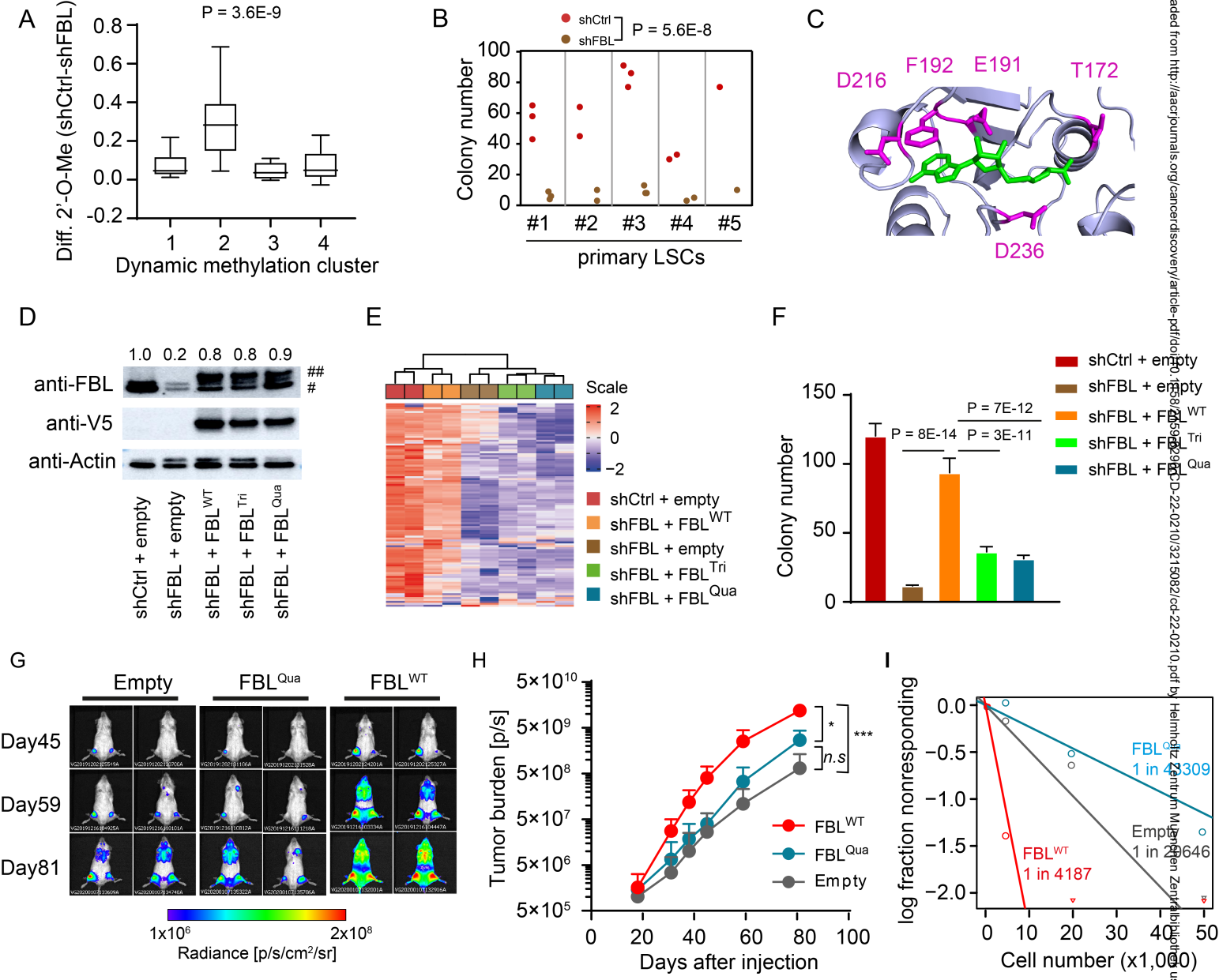

Figure 2

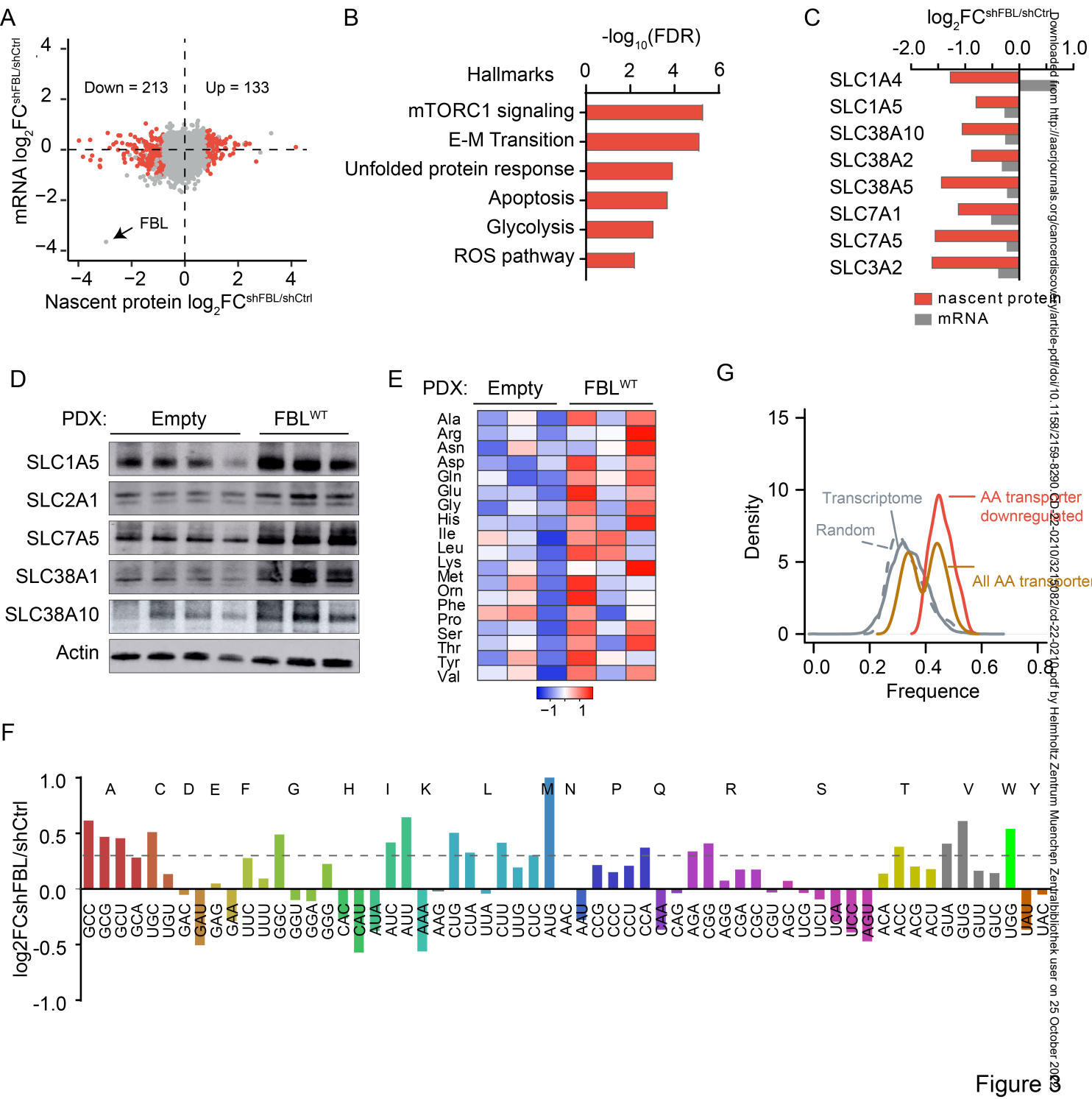

Figure 3

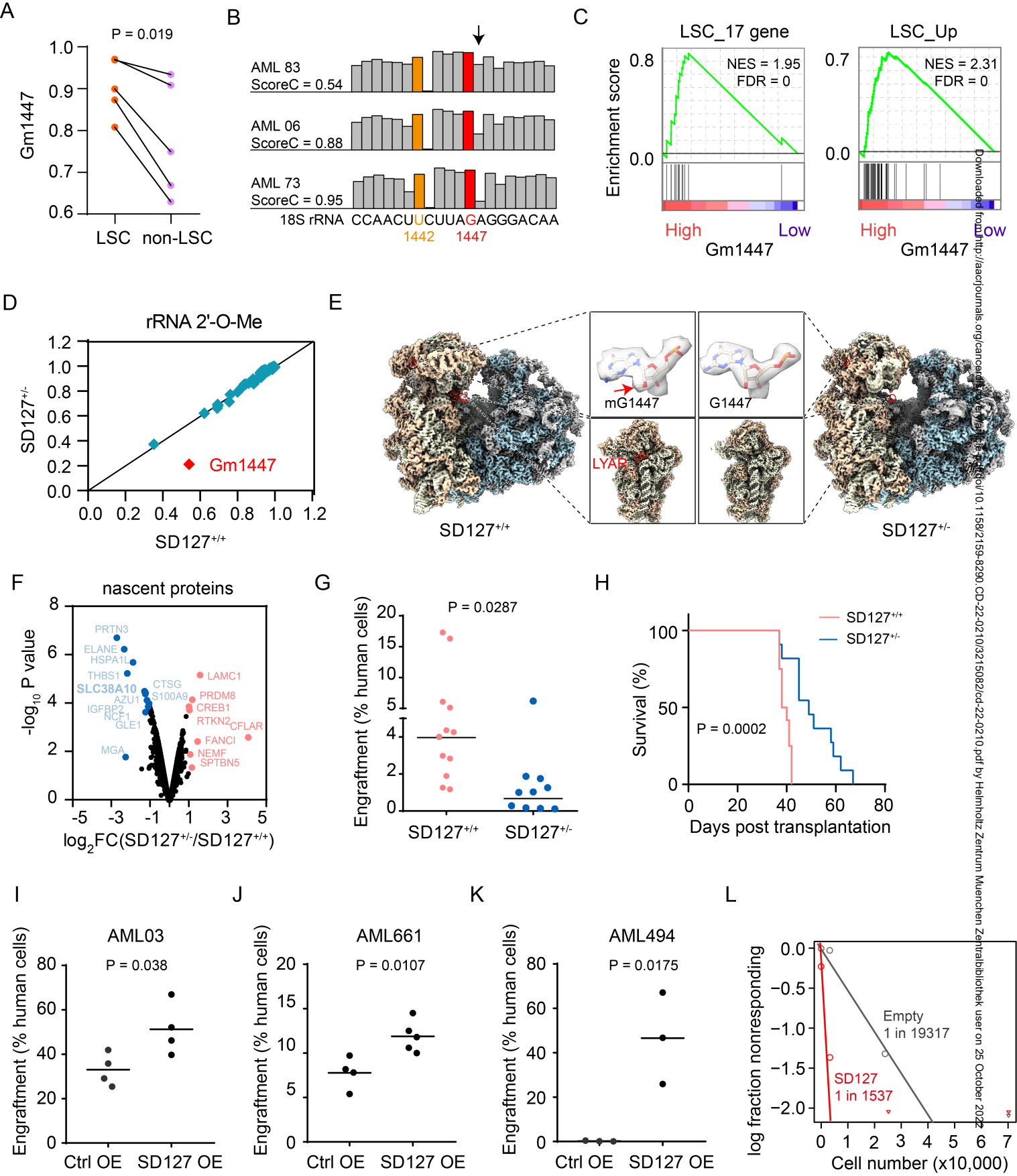

Figure 4